Energy Harvesting from Wind-Induced Vibration of Suspension Bridges

by

Miao Shi

Bachelor of Engineering (Civil)
Nanyang Technological University, 2012

Submitted to the Department of Civil and Environmental Engineering
in Partial Fulfillment of the Requirements for the Degree of

MASTER OF ENGINEERING
in Civil and Environmental Engineering
at the
Massachusetts Institute of Technology
June 2013

Signature of Author: _____

Department of Civil and Environmental Engineering
May 10, 2013

Certified by: _____

Jerome J. Connor
Professor of Civil and Environmental Engineering
Thesis Supervisor

Accepted by: _____

Heidi M. Nepf
Chair, Departmental Committee for Graduate Students

Energy Harvesting from Wind-Induced Vibration of Suspension Bridges

by

Miao Shi

Submitted to the Department of Civil and Environmental Engineering in May 10, 2013, in Partial Fulfillment of the Requirements for the Degree of Master of Engineering in Civil and Environmental Engineering

Abstract

Recently, an extensive amount of research has been focused on energy harvesting from structural vibration sources for wireless self-powered microsystem applications. One method of energy harvesting is using electromagnetic mechanism to transfer mechanical energy into electrical energy. This has been studied in depth at the micro-level scale.

In this thesis, using the same methodology that was developed for the micro-level scale, this technique is expanded for larger scale applications. A linear resonant device of the size 40mm in diameter, weight of 2 kg is proposed to be installed on a suspension bridge deck to harvest energy and to control the motion of the bridge deck. The feasibility of the installation of the device is studied with respect to the amount of energy that could be harvested. The commercial software SAP2000 was used to carry out the analysis of the structural response of the suspension bridge to wind loading. Furthermore, the potential amount of energy that can be harvested is calculated.

Keywords: Electromagnetic Energy Harvesting; Suspension bridge; Low frequency energy harvesting; Vibration control;

Thesis Supervisor: Jerome J. Connor

Title: Professor of Civil and Environmental Engineering

Acknowledgement

I would like to express my deep and sincere gratitude to my advisor, Professor Connor, not only for the precious suggestions and insightful comments for my thesis, but also the invaluable guidance and encouragement throughout my master of engineering program.

Moreover, I would like to thank Pierre, Lauren, Kris and many other staff members for their help and support. Without whom, my life would have been difficult.

Last but not least, special thanks to my parents in China for supporting me in all aspects.

Miao Shi

Contents

List of Figures

List of Tables

Chapter 1 Introduction

1.1 Background

Faced with the over-exploitation of natural resources that is associated with fast economic and demographic growth, the idea of sustainable development has been proposed since 1970s and been emphasized over the years. Sustainable development is defined as a way of development that fulfills the present needs without sacrificing the future (Meadows, Randers, & Behrens, 1972). This is possible through rational management among human, nature and economics.

Moreover, with the global warming effect, an urge to cut down on the carbon foot print has been encouraged worldwide. This requires the replacement and retrofit of current energy methods with ones that do not emit carbon dioxide, which is often referred to as alternative energy.

According to the records (U.S. Energy Information Administration (EIA) International Energy Statistics , 2010), 84% of the energy consumption today is due to fossil fuel. It is predicted that the fossil fuel stored can only last for another 100 years if we do not change the way of generating energy. Therefore, according to British Petroleum and Royal Dutch Shell (Shell says record profits to be used to boost alternatives, 2006), by 2050, one-third of the world's energy will need to come from alternative energy sources, which is the only way we can survive beyond the 21st century.

Alternative energy sources include biomass energy, wind energy, solar energy, geothermal energy, hydroelectric energy, and mechanical vibration energy sources. The latter, mechanical vibration, is an attractive energy source for certain circumstances. The idea of energy harvesting using Micro-Electro-Mechanical System (MEMS) has been developed during the last couple of decades, with the development of miniaturized systems with micro sensors placed on the structure. These sensors can provide information about the health state of the structure, so that monitoring and controlling are feasible. For example, an array of sensors can be applied to the bridge to assess its structural health. But to perform such an assessment, the sensors need to be powered to send signals to the bridge structure and to send the data back to the monitoring center. The MEMS makes it possible to let the sensors work without fixed power source and without the use of batteries. The vibration or the mechanical motion of the structure has been the major driving source for the MEMS.

The design concept of suspension bridge is able to provide people with longer clear spans, but it also creates a lot of engineering difficulties, like controlling the vibration and fatigue failure of the structure. The suspension bridge structure is relatively slender compared to other infrastructures, which may result in larger deflection and structural vibration response. The wind, moving vehicles are a few major sources that cause the structure to vibrate vigorously. More specifically, wind can result in catastrophic failure of the structure.

The feasibility of harvesting energy from a suspension bridge and controlling the motion of the bridge deck concurrently are studied in this thesis.

1.2 Objective

Using electromagnetic energy harvesting devices, the feasibility of harvesting energy from a suspension bridge is studied. The objective of this thesis is to determine how much energy that can be harvested from the oscillation of the bridge under wind loading.

The focus of this study is on harvesting energy from wind induced vibration on the bridge deck, which is characterized by its low frequency. The existing electromagnetic harvesting devices are usually used for a high frequency range. To maximize the energy output, a device characterized by its low natural frequency is established to satisfy the specific frequency requirements. In addition, the potential energy that could be harvested is determined. This study is expanded by applying a larger number of such devices to the suspension bridge. Finally, the effect of these devices on damping was further studied with respect to energy harvesting.

The relationship between the wind speed and structural response was also studied, in order to establish the relation between the wind speed and the potential energy harvested.

Chapter 2 Literature Review

2.1. Energy Harvesting Devices

2.1.1. Introduction

Energy has been gathered from natural environment and turned into use since a long time ago, when machineries like windmills and waterwheels were invented. Over the past few decades, driven by the increasing need to power remote electrical sensor networks and movable devices, the idea of extracting electrical energy from the operating environment has attracted many researchers' attention. At the same time, the problem of global warming, which requires lowering the carbon foot print, lead to searching for alternative energy.

There is a wide range of sources where energy can be harvested from: mechanical, solar, chemical, ambient-radical or the combination of them. In this thesis, the focus is on the mechanical vibration sources (Chalasani, 2008).

To harvest kinetic energy from the environment, the generator requires two parts (refer to Figure 1). First, a vibration mechanical system should be set up to turn environmental motion into the generator's motion. Second, a transduction mechanism should be used to turn the kinetic energy into electrical energy (Williams & Yates, 1996). The design of the mechanical system should maximize the coupling effect of the kinetic energy source and the transduction mechanism. Typical vibration-powered generators are with inertial spring and mass system, along with damping effect which is related to the transduction mechanism.

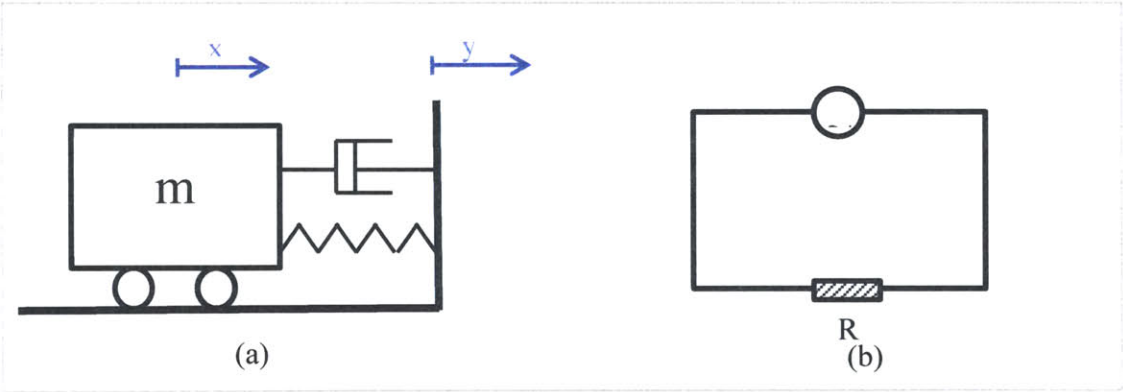

Figure 1 Schematics of (a) Mechanical System and (b) Electrical transduction System

2.1.2. Transduction Energy Mechanism

During the past decades, three main energy transduction mechanisms have been developed:

❖ Smart Materials Energy Harvesting

Smart materials are designed to have one or more properties that can change significantly by inducing stress, temperature, moisture, pH, electric or magnetic fields (Wikipedia, 2013). Mechanical vibration causes continuous change in the stress of the material, which can produce electrical energy. The following are some of the smart materials that can be used for harvesting energy from vibration.

- Piezoelectric (PZT) materials

  PZT are materials that produce a voltage when the strain is induced in across the materials. Since the late 1990's, a vibration-powered micro-generator based on a screen printed PZT has been proposed by White, Glynne-Jones, and Beeby for the remote sensor systems as an alternative energy source. With a excitation frequency of 80Hz, numerical calculations and experimental studies show that $2\,\mu W$ of energy is generated. Subsequently, a number of researchers devoted for optimizing and extending the usage of PZT energy harvesting. In 2006, a battery-free wireless doorbell push button was invented (World's First Batteryless Wireless Doorbell, 2006). Since the 21st century, new technology has been applied to the industry to harvest energy from vibration or shock (Energy harvesting). Furthermore, PZT elements can be embedded in walkways to harvest energy from people walking.

  The PZT material remains an emerging technology with new breakthrough innovations. In 2005, a thin film PZT, MEMS power generating device is created by MIT researchers which increases the energy output with low resonant frequency (Jeona, Sood , Jeong, Kim, 2005). By introducing non-linearity into the stiffness of a doubly clamped Micro-Electro-Mechanical systems resonator, an ultra-wide-bandwidth energy harvester was created by Hajati and Kim, which increases the range of frequency and the amount of energy that can be harvested (Hajati & Kim, 2011).

- Electro-active-polymers (EAPs)

  This new type of polymer has come to the field of energy harvesting. The advantages of the materials are:
  - Large strain
  - Elastic energy density
  - High efficiency to convert mechanical energy
  - Light weigh

❖ Electrostatic (capacitive) energy harvesting

This type of mechanism is based on the variation of the capacity due to the movement of the plates. The capacity change causes movement of the electrons in the circuits (refer to Figure 2). The energy is extracted from moving the plates against electrostatic force.

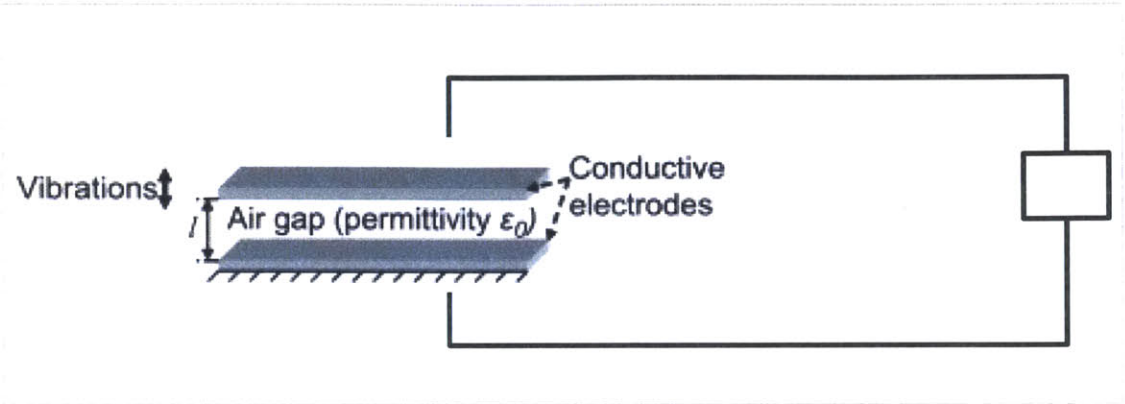

Figure 2 Electrostatic Energy Harvester (Lallart, Pruvos and Guyomar, 2011)

- Electromagnetic energy harvesting

  The electromagnetic energy harvesting mechanism is based on the Faraday's Law of induction. The relative movement caused by vibration results in the change of magnetic flux in the coil; thus, an electric current is generated in the coil. The size of the magnet and the number of turns of the coil dominates the energy output if the vibration is held constant, which also determines the size of the harvester. In this thesis, the Electromagnetic energy generator is used.

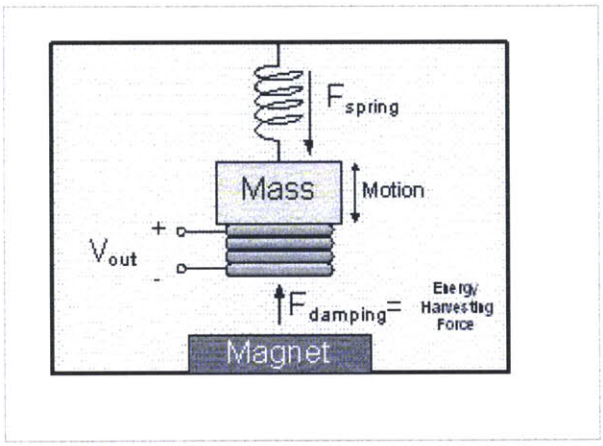

Figure 3 Electromagnetic Energy Harvester

(Energy-harvesting chips: The quest for everlasting life, 2005)

2.1.3. Resonant vibration Transducer Theory

When modeling the Energy harvester, earlier research focused on the response of "Linear resonance (LR)" devices subjected to sinusoidal excitation. Later because of the limitation of the LR device, nonlinear resonance became more interesting to the researchers.

❖ Linear Resonant (LR) Device

In 1996, a Single-Degree-of-Freedom (SDOF) mass-spring-damper system was proposed (Williams & Yates, 1996), as shown in Figure 4.

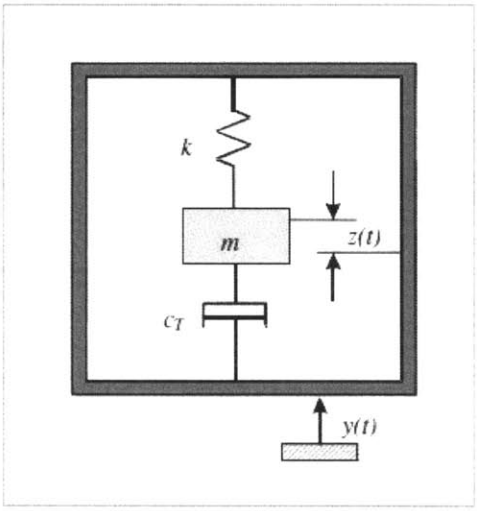

Figure 4 Mechanical Model of a Linear, Inertial Generator (Williams and Yates, 1996)

The generator is a simple mass-spring mechanical system placed inside a rigid frame, with a mass (m), a spring of stiffness k, and a damper of damping coefficient c. The energy lost through damping within the system is categorized into two parts: parasitic loss (damping coefficient c_m) and harvested electrical energy (damping coefficient c_e). The net displacement between the mass and the frame is denoted as z in equation 2.1.1. Assuming the mass m is significantly smaller than the source mass, the source is not affected by its presence, and the equation of motion can be described as

$$m\ddot{z} + c\dot{z} + kz = -m\ddot{y} \qquad \textbf{2.1. 1}$$

In Equation (2.1.1), the external vibration y is described by

$$y = Y sin(\omega t) \qquad \textbf{2.1. 2}$$

Solving the differential Equation (2.1.1) by substituting Equation (2.1.2), the steady state solution is described by

$$z = \frac{\omega^2}{\sqrt{(\frac{k}{m} - \omega^2)^2 + (2\zeta_T \omega)^2}} Y sin(\omega t - \varphi) \qquad \textbf{2.1. 3}$$

Where, $\varphi = tan^{-1}(\frac{c_T\omega}{k\omega^2 m})$

$$\zeta = \frac{c}{2m\omega_n}$$

From Equation (2.1.3), the maximum energy can be harvested when $\omega = \omega_n = \sqrt{\frac{k}{m}}$.

The total power dissipated in the damper is shown as

$$P_d = \frac{m\zeta Y^2(\frac{\omega}{\omega_n})^2\omega^3}{[1-(\frac{\omega}{\omega_n})^2]^2 + [2\zeta\left(\frac{\omega}{\omega_n}\right)]^2} \quad \textbf{2.1.4}$$

When $\omega = \omega_n = \sqrt{\frac{k}{m}}$, maximum power output is

$$P_d = \frac{mY^2{\omega_n}^3}{4\zeta} \quad \textbf{2.1.5}$$

Denoting $A = {\omega_n}^2 Y$, Equation (2.1.5) can be written as

$$P_d = \frac{mA^2}{4\zeta\omega_n} \quad \textbf{2.1.6}$$

Then the maximum power can be calculated by

$$P_e = \frac{m\zeta_e A^2}{4\omega_n(\zeta_m+\zeta_e)^2} \quad \textbf{2.1.7}$$

From Equation (2.1.7), P_e is proportional to m. Since ζ_p is always larger than zero in reality, the maximized P_e can be achieved by adjusting ζ_m and ζ_e (Beeby, Tudor, & White, 2006).

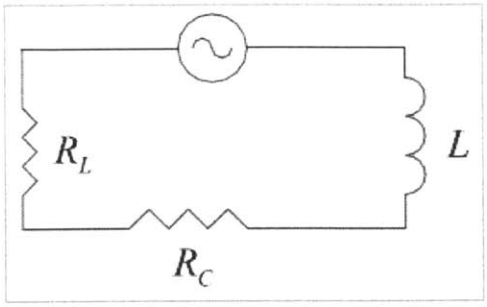

Figure 5 Electrical Transduction System (Williams and Yates, 1996)

The electric transduction mechanism is simplified as shown in Figure 5.

Where, R_L represents load resistant (in ohms), R_c represents coil resistant (in ohms) and L is coil induction (in ohms).

The electromagnetic transduction c_e can be estimated as

$$c_e = \frac{(\boldsymbol{NlB})^2}{R_L + R_c + L} \qquad \textbf{2.1. 8}$$

Coil induction is relatively small compared to the load and coil resistance, hence L can be ignored in the equation and Equation (2.1.7) is simplified to

$$c_e = \frac{(\boldsymbol{NlB})^2}{R_L + R_c} \qquad \textbf{2.1. 9}$$

Since mechanical damping is unavoidable, with further mathematical optimization, it is shown that when $\zeta_p = \zeta_e$, P_e can be maximized.

By equalizing ζ_p and ζ_e, optimum R_L that maximizes $P_e$can be determined:

$$R_L = R_c + \frac{(NlB)^2}{c_m} \qquad \textbf{2.1. 10}$$

The LR device has the limitation of being excited only near its resonance frequency, which results in the narrow-band performance. Consequently, it cannot harvest energy from a broadband excitation or changing dominant frequencies, which are the features of dominant excitation from the environment.

❖ Nonlinear Resonant Device

Introducing dynamic nonlinearities into the system will increase the range of excitation frequencies of the device. Mann BP and Sims ND (2009) studied a levitated magnetic energy harvesting device, which behaves like the mono-stable hardening spring Duffing

Oscillator (refer to Figure 6). Following the same device model, Green et al. (2012) showed that by using mono-stable energy harvester, it is possible to have a smaller energy harvesting device with similar energy output, and extending the bandwidth of the effective performance.

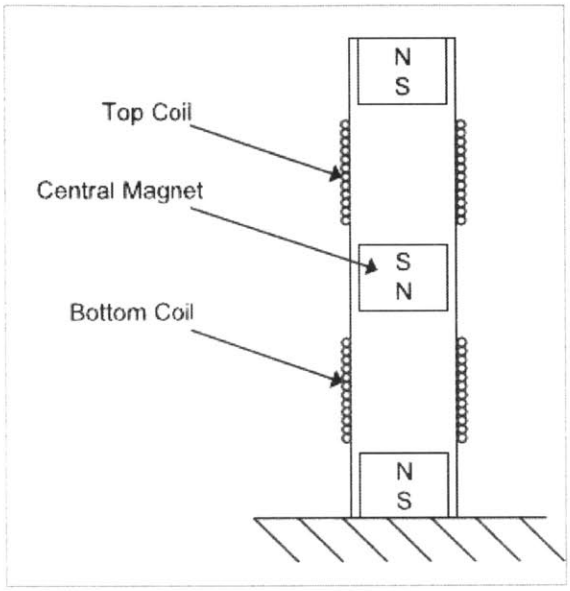

Figure 6 Schematic Diagram of Mono-Stable Energy Harvester (Mann and Sims, 2009)

The model to harvest energy from the magnetic levitation can be simplified into a mass damper system as shown in Figure 7.

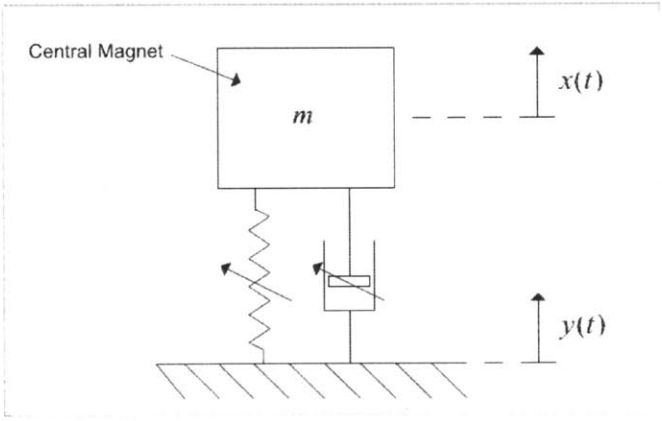

Figure 7 Energy Harvester Model (Mann and Sims, 2009)

(Green et al. 2012) Denoting $z = x - y$, the equation of motion can be written as:

$$m\ddot{z} + c\dot{z} + F_d sgn(\dot{z}) + kz + k_3 z^3 + F_e = -m\ddot{y} \qquad \textbf{2.1. 11}$$

Where,

m: mass of the central magnet

c: viscous mechanical damping coefficient

k: linear stiffness

k_3: Nonlinear Stiffness

F_e: Direct current force due to electromagnetic coupling

F_d: Coulomb damping coefficient due to friction

$y = Ysin(\omega t + \varphi)$

$z = Zsin(wt)$

F_e can be neglected due to the fact it is much smaller than the rest of the forces. Then the equation of motion can be written as:

$$m\ddot{z} + c\dot{z} + F_d sgn(\dot{z}) + kz + k_3 z^3 = -m\ddot{y} \quad \textbf{2.1. 12}$$

In Equation (2.1.12), the coefficient of coulomb damping F_d can be expanded using Fourier series:

$$sgn(\cos(\omega t)) = \frac{4}{\pi}\cos(\omega t) - \frac{4}{3\pi}\cos(3\omega t) + \frac{4}{5\pi}\cos(5\omega t) + \cdots \quad \textbf{2.1. 13}$$

Using the accuracy for the first harmonic degree, the equation is simplified to

$$sgn(\cos(\omega t)) \approx \frac{4}{\pi}\cos(\omega t) \quad \textbf{2.1. 14}$$

The coefficient of $k_3$is expanded based on elementary trigonometric relations

$$Z^3\sin^3(\omega t) = Z^3(-\frac{1}{4}\sin(3\omega t) + \frac{3}{4}\sin(\omega t)) \quad \textbf{2.1. 15}$$

If the first harmonic accuracy is also used, the term can be written as:

$$Z^3\sin^3(\omega t) \approx Z^3\frac{3}{4}\sin(\omega t) \quad \textbf{2.1. 16}$$

Consequently, the equation of motion becomes

$$-m\omega^2 Z sin(wt) + c\omega Z cos(wt) + F_d s\frac{4}{\pi}\cos(\omega t) + kZ sin(wt) + k_3 Z^3[\frac{3}{4}\sin(\omega t)] = -m\omega^2 Y(sin(wt)\cos(\varphi) + \cos(\omega t)\sin(\varphi)) \quad \textbf{2.1. 17}$$

By equalizing the terms of $sin(wt)$ and $cos(wt)$, the following two equations can be extracted:

$$-m\omega^2 Z + kZ + \frac{3}{4}k_3 Z^3 = m\omega^2 Y cos(\varphi) \quad \textbf{2.1. 18}$$

$$c\omega Z + \frac{4}{\pi}F_d = m\omega^2 Y cos(\varphi) \quad \textbf{2.1. 19}$$

Knowing that $sin^2(\varphi) + cos^2(\varphi) = 1$,

$$\left[-m\omega^2 Z + kZ + \frac{3}{4}k_3 Z^3\right]^2 + \left[c\omega Z + \frac{4}{\pi}F_d\right]^2 = m^2\omega^4 Y^2 \quad \textbf{2.1. 20}$$

With further derivation of the above equation,

$$Z^6\left(\frac{9k_3}{16}\right) + Z^4\left(-\frac{3}{2}m\omega^2 k_3 + \frac{3}{2}kk_3\right) + Z^2(m^2\omega^4 - 2m\omega^2 k + k^2 + c^2\omega^2) + Z\left(\frac{8c\omega F_d}{\pi}\right) + \left(\frac{16{F_d}^2}{\pi^2} - m^2\omega^4 Y^2\right) = 0 \quad \textbf{2.1. 21}$$

By solving the above equation Z can be determined.

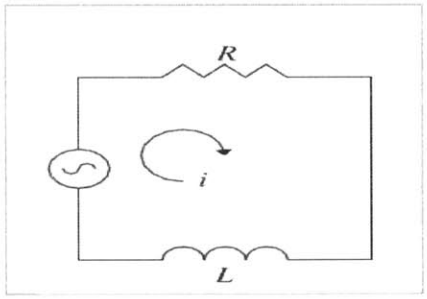

Figure 8 Circuit Diagram of the Magnetic Levitation Energy Harvester (Green et al 2012)

The electromagnetic transduction part of the harvester can be modeled as a closed circuit as shown in Figure 8.

The relationship between the components can be written as:

$$V(t) = I(t)R + \frac{dI(t)}{dt}L \quad \textbf{2.1. 22}$$

Where,

R: the combined resistance of coil and load

L: coil induction

I(t): Current

From Faraday's Law, the voltage can be generated by

$$V(t) = Blz(\dot{t}) \quad \textbf{2.1. 23}$$

Where,

$V(t)$: Induced voltage

B: Average magnetic strength over the target area

l: Length of the coil wire

From Lorentz's Law, and assuming constant electromagnetic flux over the target area, the force applied on the magnet can be expressed as

$$\mathrm{F(t)} = \mathrm{BI(t)l} \quad \textbf{2.1. 24}$$

Using Laplace transform,

$$\mathcal{L}\big(F(t)\big) = \frac{s(Bl)^2 L(z(t))}{R + sl} \quad \textbf{2.1. 25}$$

Where,

s: Laplace operator

Assuming that the inductance is much smaller than the resistance, a viscous damper can be modeled as the transducer, with a damping coefficient of $c = \frac{(Bl)^2}{R}$.

Further, assuming the viscous damping in the system is due to the electromagnetic coupling, the power output of the device can be written as

$$P = c(\dot{z})^2 \quad \textbf{2.1. 26}$$

2.2. Electromagnetic Knowledge

2.2.1 Magnetic forces

Permanent magnets are used in the electromagnetic energy harvesting devices. Knowledge of the magnetic force is necessary to design and control devices. Vokoun et al (2009) proposed

the Euqation (2.2.1) to calculate the force between two identical cylindrical magnets with their center line aligned.

$$F(s) = \frac{\pi B_0^2}{\mu_0} R^4 [\frac{1}{s^2} + \frac{1}{(s+2h)^2} - \frac{2}{(s+h)^2}] \quad \text{2.2. 1}$$

Where,

s: Distance between the cylinders

h: cylinder radius

h: cylinder height

2.2.2 Magnetic field

A magnetic field describes the magnetic influence of electric currents and magnetic materials to the space. The force between the two magnetized surfaces can be expressed using magnetic field strength:

$$F = \frac{AB^2}{2\mu_0} \quad \text{2.2. 2}$$

Where:

A: the area of each surface

μ_0: is the permeability of space, which equals $4\pi \times 10^{-7}$ T·m/A

B: is the flux density

2.3. Suspension Bridge

2.3.1 Introduction to suspension bridge

Suspension bridges are widely used and have existed for many years. The earliest suspension bridges were built in the 15th century outside Tibet and Bhutan Area (Gerner, 2007). People took advantages of the tension of the tailing plants like vines, creeps to make ropes from them. The idea of suspension bridge is vastly adopted in mountainous area around the world since 19th century.

Metals materials have been replacing the use of natural materials, and this was also applied to suspension bridges. Retaining the concept of using tension elements to support the vertical loadings, the natural ropes are replaced by iron chains- building the first chain bridge in England in 1741. Modern days, the span of the bridge has been extended by using wire cables and new technology. The longest suspension bridge today is Akashi Kaikyō Bridge, located in Japan, with a main span of 1991 meters (Cooper, 1998).

Because of lack of stiffness of the suspension bridge, the analysis approach is different. Besides the updated elastic and deflection analysis of the suspension bridge, the aerodynamic stability of the bridge has caught engineers' attention after several major failures of suspension bridges.

2.3.2 Components of a Suspension Bridge

Figure 9 shows the typical components of a suspension bridge, consisting of a parabolic main cable and vertical hangers connecting to the deck. The three-span suspension bridge is the most common suspension bridge system which consists of equal and symmetrical side spans.

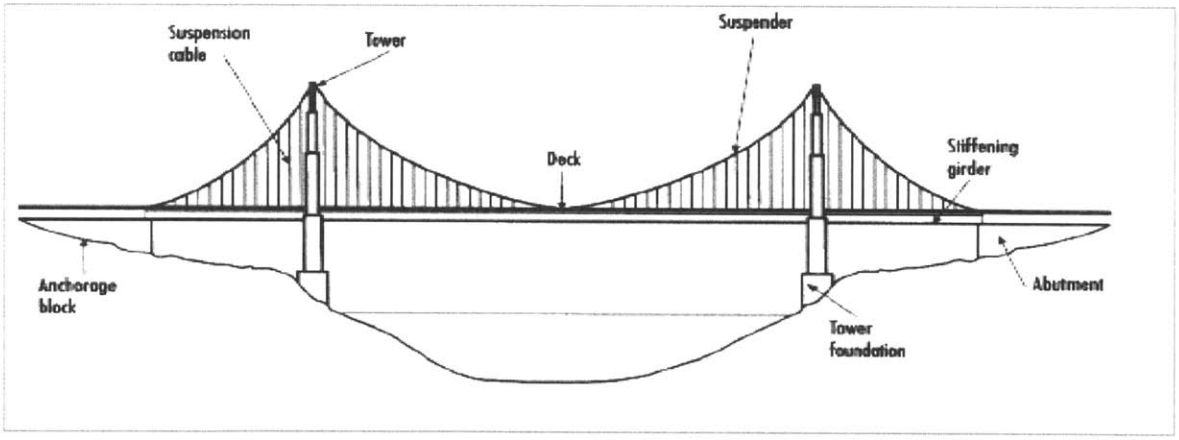

Figure 9 Main Components of Suspension Bridge (Suspension Bridge Diagram)

Figure 10 displays the structural components of a typical suspension bridge system, with its superstructure and substructure.

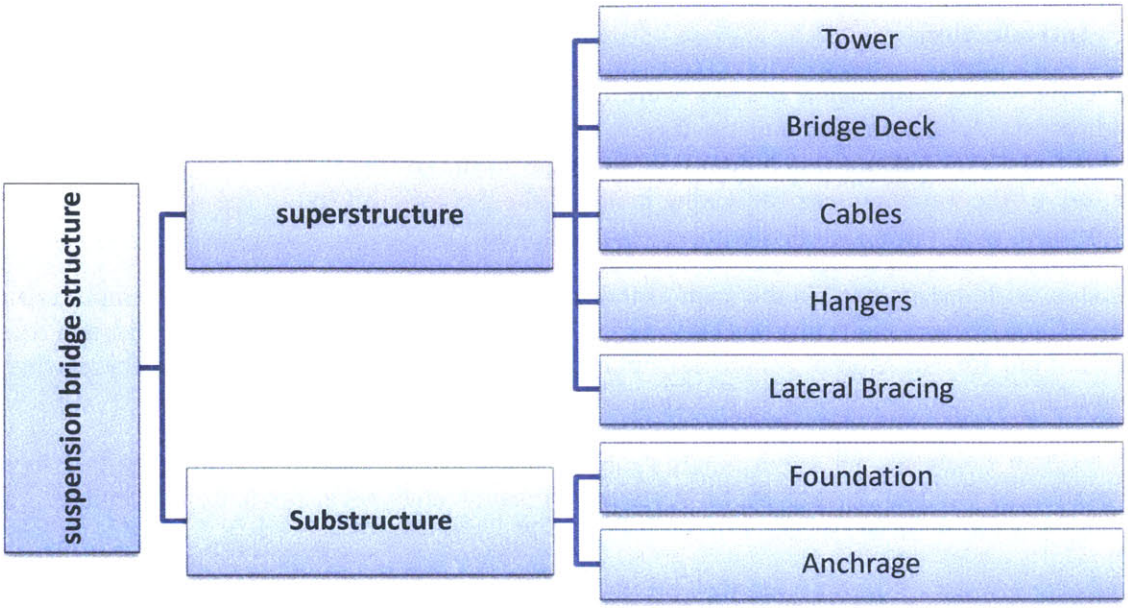

Figure 10 Suspension Bridge System

Four main componets of the suspension bridge are identified in (Gimsing and Georgakis, 2012).

- The deck/stiffening girder
- The cable system
  It is used to support the deck.
- The pylons/towers
  It is used to support the cable system.
- The anchorage blocks
  It is used to support the cable system vertically and horizontally at the ends

2.4. Wind Effect

2.4.1 Introduction

In the early years, suspension bridges were designed for drag forces and the forces along the wind direction. John Roebling was the first to identify the dynamic response of the bridge under wind load in 1855, but not much attention was paid to the dynamic effect. Until the tragedy of the failure of the Tacoma Narrow Bridge in 1940, the dynamic effects of the wind on the decks of the bridges were paid enough attention. (Holmes, 2007)

Nowadays, with the increase in the span of the suspension bridge, the wind effect is more critical in the design. The resonant response of the bridge can be excited by several modes due to the dynamic wind forces. Moreover, the aero-elastic forces which are self-generated forces due to motion of the structures can lead to a critical scenario.

The wind can excite the vibration of the cables and deck of a suspension bridge. In this thesis, the vibration of the deck is studied. First, the aerodynamic analysis of the deck is introduced and the analysis is based on the model shown in Figure 11.

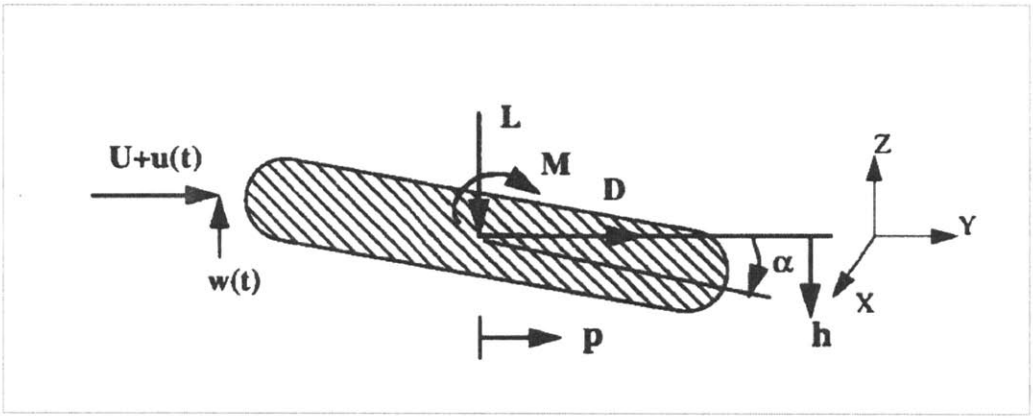

Figure 11 Wind Force on the Bridge Deck Cross Section

The terms show in Figure 11 are:

M:	Mass per unit length
I:	Moment of inertia
c_z, c_y, c_α:	Damping coefficient
s_z, s_y, s_α:	Stiffness coefficient
U:	mean wind speed

$u(t)$: Fluctuation in horizontal direction

$w(t)$: Fluctuation in z direction

D: Horizontal Force / unit length

L: Vertical Force / unit length

M: Moment / unit length

z: Vertical deflection

y: Horizontal deflection

α: Torsional deflection

The equation of motion of the structural element shown in Figure 11 can be presented as:

$$m\ddot{z} + c_z\dot{z} + s_z z = L \quad \textbf{2.3.1}$$

$$m\ddot{y} + c_y\dot{y} + s_y y = D \quad \textbf{2.3.2}$$

$$I\ddot{\alpha} + c_\alpha\dot{\alpha} + s_\alpha\alpha = M \quad \textbf{2.3.3}$$

Equations (2.3.1), (2.3.2) and (2.3.3) are equivalent to the following:

$$L = m(\ddot{z} + 2\zeta_z w_z\dot{z} + w_z^2 z) \quad \textbf{2.3.4}$$

$$D = m(\ddot{y} + 2\zeta_y w_y\dot{y} + w_y^2 y) \quad \textbf{2.3.5}$$

$$I = I(\ddot{\alpha} + 2\zeta_\alpha w_\alpha\dot{\alpha} + w_\alpha^2\alpha) = L \quad \textbf{2.3.6}$$

Where,

$\zeta_z, \zeta_y, \zeta_\alpha$: Mechanical damping

$\omega_z, \omega_y, \omega_\alpha$: Natural frequency

From Theodorsen's Expansion for lift & moment on flat plates (Theodorsen, 1934), assuming that the flow is always attached; the object can be analyzed as a flat plate; and the wake is flat, the lift and moment of the object can be written as

$$L = \pi\rho UBC(h)\left(\dot{z} + Uz + \frac{B}{4}\dot{\alpha}\right) - \frac{\pi}{4}\rho B^2(\ddot{z} + U\dot{\alpha}) \quad \textbf{2.3.7}$$

$$M = \frac{\pi}{4}\rho UB^2C(h)\left(\dot{z} + Uz + \frac{B}{4}\dot{\alpha}\right) - \frac{\pi}{16}\rho B^3\left(\frac{\pi}{16}\ddot{\alpha} + U\dot{\alpha}\right) \quad \textbf{2.3.8}$$

Where,

B: Half of bridge width

U: Mean wind speed

h: $\frac{\omega B}{U}$

$C(h)$: Theodorsen's Function

Because of the low density of the air, the mass and moment of inertia can be ignored, Equation (2.3.7) and (2.3.8) can be written as:

$$L = \rho U^2 B \left(h H_1^* \frac{\dot{z}}{U} + h H_2^* \frac{B}{U} \dot{\alpha} + h^2 H_3^* \alpha \right) \quad \textbf{2.3. 9}$$

$$M = \rho U^2 B^2 \left(h A_1^* \frac{\dot{z}}{U} + h A_2^* \frac{B}{U} \dot{\alpha} + h^2 A_3^* \alpha \right) \quad \textbf{2.3. 10}$$

Assuming the bridge deck acts as a wind tunnel, torsional motion is restrained, α is zero. The lift force described in Equation (2.3.9) can be simplified to:

$$m(\ddot{z} + 2\zeta_z w_z \dot{z} + w_z^2 z) = \rho U^2 B \left(h H_1^* \frac{\dot{z}}{U} \right) \quad \textbf{2.3. 11}$$

Substituting $z = z_0 e^{\alpha t} \sin wt$ into Equation (2,3,11), the equation becomes

$$\left(\alpha^2 - w^2 + 2\zeta_z w_z \alpha + w_z^2 - \frac{\rho U B h H_1^*}{m} \right) \sin wt + 2\alpha \cos wt = 0 \quad \textbf{2.3. 12}$$

Where,

$$H_1^* = \frac{m}{\rho w B^2} 2(\alpha + \zeta_z w_z) = \frac{m}{\rho w a B^2} 2(\alpha^2 - w^2 + 2\zeta_z w_z \alpha + w_z^2) \quad \textbf{2.3. 13}$$

2.4.2 Bridge Deck Oscillation due to Wind

There are three major mechanisms that can oscillate the bridge deck at resonance, which depends on the wind velocity. The dynamic response varies with the magnitude of the wind velocity, and the relation between the wind velocity and the response of the structure is shown in Figure 12.

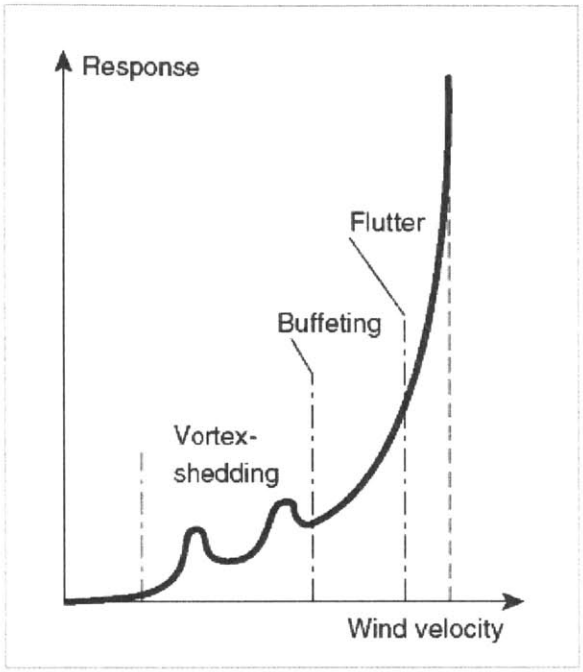

Figure 12 Dynamic Response of a Slender Bridge Structure under Wind Action

(Gimsing & Georgakis, 2012)

❖ Flutter instability

Despite the fact that the deck may be aerodynamically stable, under very large wind velocity flutter instability occurs. This is due to the domination of the aerodynamic forces from self-excitation. Flutter instability will always cause torsion in the bridge deck and possible vertical movement.

Lift (L_{se}), drag (D_{se}) and Moment (M_{se}) caused by self-excitation:

$$L_{se}(t) = \frac{1}{2}\rho\bar{U}^2 B[KH_1^*\frac{\dot{h}}{\bar{U}} + KH_2^*\frac{B\dot{\alpha}}{\bar{U}} + K^2H_3\alpha] \quad \text{2.3. 14}$$

$$D_{se}(t) = \frac{1}{2}\rho\bar{U}^2 B[KP_1^*\frac{\dot{h}}{\bar{U}} + KP_2^*\frac{B\dot{\alpha}}{\bar{U}} + K^2P_3\alpha] \quad \text{2.3. 15}$$

$$M_{se}(t) = \frac{1}{2}\rho\bar{U}^2 B[KA_1^*\frac{\dot{h}}{\bar{U}} + KA_2^*\frac{B\dot{\alpha}}{\bar{U}} + K^2A_3\alpha] \quad \text{2.3. 16}$$

Where,

ρ: Density of air

B: Full width of bridge deck

$K = \frac{B\omega}{U}$: Reduced frequency

H_i^*, P_i^*, A_i^*: Aero dynamic coefficient (refer to Figure 13)

$\overline{U}$: Horizontal mean wind velocity

h: Vertical displacement of the bridge deck

α: Rotational Displacement of bridge deck

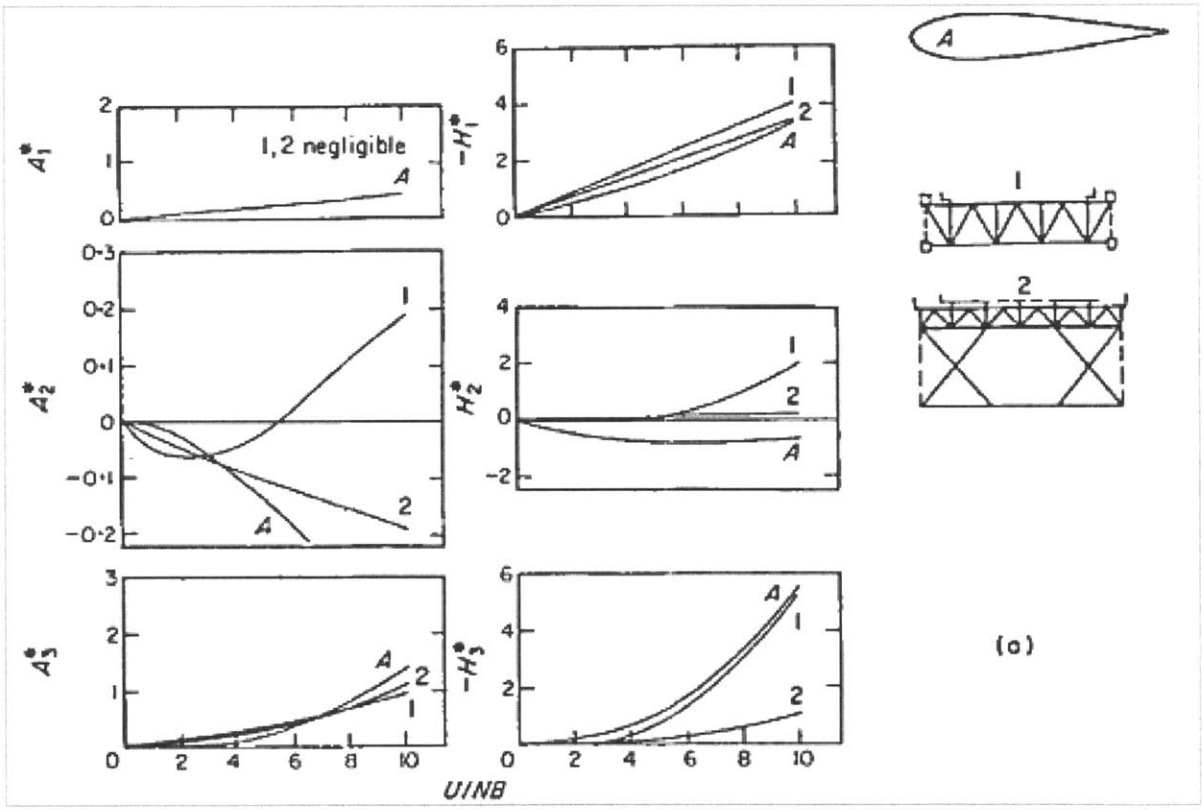

Figure 13 Examples of Representative Flutter Derivatives. (a) Thin Airfoil; 1) Trussed Deck with Instability Tendencies; 2) Stable Truss Deck. (Theodorsen, 1934)

❖ Buffeting excitation

The fluctuating forces induced by the turbulence, result in the suspension bridge undergoing buffeting excitation. It usually occurs over a relatively larger range of wind speeds (Scanlan R. H., 1978).

$$L(t) = L_{se}(t) + L_b(t) \quad \text{2.3. 17}$$

$$D(t) = D_{se}(t) + D_b(t) \quad \text{2.3. 18}$$

$$M(t) = M_{se}(t) + M_b(t) \quad \text{2.3. 19}$$

Where,

L_{se}, D_{se}, M_{se}: Lift, drag and moment due to self-excitation motion

L_b, D_b, M_b: Lift, drag and moment due to buffeting effect;

$$L_b(t) = \frac{1}{2}\rho\bar{U}^2 B\{C_L(0)\left[1 + \frac{2u(t)}{\bar{U}}\right] + \left[\frac{dC_L(0)}{d\alpha} + C_D(0)\right]\frac{w(t)}{\bar{U}}\} \quad \text{2.3. 20}$$

$$D_b(t) = \frac{1}{2}\rho\bar{U}^2 B\{C_D(0)\left[1 + \frac{2u(t)}{\bar{U}}\right]\} \quad \text{2.3. 21}$$

$$M_b(t) = \frac{1}{2}\rho\bar{U}^2 B\{C_M(0)\left[1 + \frac{2u(t)}{\bar{U}}\right] + \left[\frac{dC_M(0)}{d\alpha}\right]\frac{w(t)}{\bar{U}}\} \quad \text{2.3. 22}$$

Where,

$C_L(0), C_D(0), C_M(0)$: Dimensionless coefficient

$u(t)$: Wind velocity in the horizontal direction

$w(t)$: Wind velocity in the vertical direction

❖ Vortex-Shedding Excitation

The vortex-shedding excitation often happens with the condition of low wind speed and low turbulence condition (Holmes, 2007).

$$F(t) = \rho U^2 D C_L \sin(2\pi f t) \quad \text{2.3. 23}$$

Where,

ρ: Density of air

C_L: lift coefficient

D: Diameter of object

Since the bridge is modeled as a truss structure, the wind can go through it. Thus, the concentrated vortex cannot occur. Therefore, the vortex-shedding oscillation of the deck is small (Simiu, 1986).

Chapter 3 Methodology

Figure 14 describes the methodology used for this thesis. First, a suspension bridge model was built in SAP2000. Next, the wind load applied to the bridge was calculated based on the wind data collected. Then the calculated loads were applied onto the suspension bridge model to analyze the response of the structure. The electro-magnetic energy harvesting device was modeled as a mass damper system with equivalent stiffness, mass and damping coefficient. The potential energy that can be harvested is based on both the motion of the main structure and damping coefficient of the energy harvester. In addition, the change in amplitude of the wind and its effect on the oscillation amplitude of bridge was also studied as an indication of the potential energy that can be harvested.

Further numerical analysis of the array of energy harvesting devices and their effect on the main structure was based on the design of an equivalent mass damper system to achieve the target damping coefficient of the bridge. In this analysis, since the response varies along the bridge, the bridge was divided into small sections each of 30 feet in length. Thus, each section can be treated with uniform response behavior. For each section, the number of energy harvesting devices that should be used and the damping coefficient of the device can be determined. The total energy harvested is the sum of all the sections.

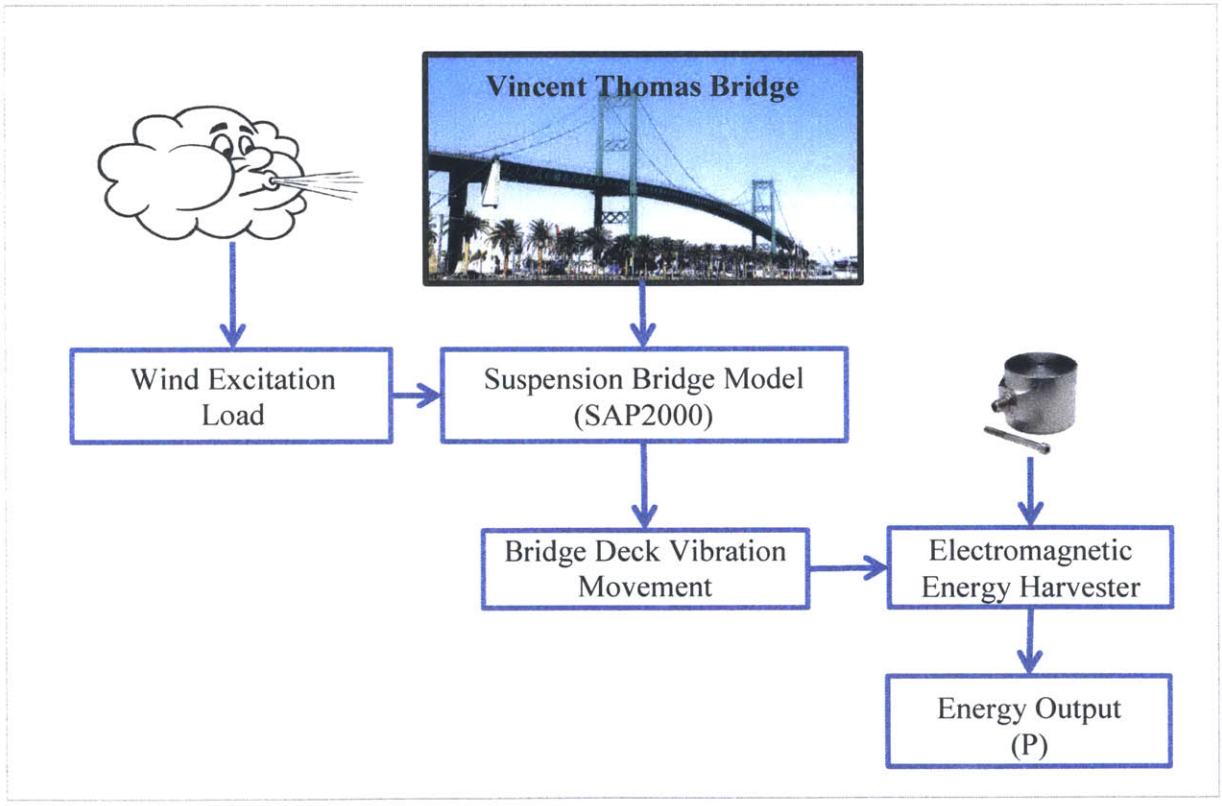

Figure 14 Methodology

Chapter 4 Suspension Bridge Analysis

4.1 Model of Suspension Bridge

The suspension bridge modeled in this thesis is based on the Vincent Thomas Bridge located in California. The Bridge has a mid-span of 1500 feet and side spans of 506.5 feet, as shown in Figure 15. The actual bridge is complex, not only in terms of the large numbers of members, but also the connections between members, such as cable bents and shear connecters. To fulfill the objective of this thesis, the suspension bridge is modeled to acquire its dynamic response. Thus, the connections are not modeled for simplicity. Only main structural elements like cables, suspenders, towers and decks are carefully modeled. Moreover, the deck and the tower structural elements are modeled carefully to provide correct bending, and torsional stiffness for the dynamic response analysis.

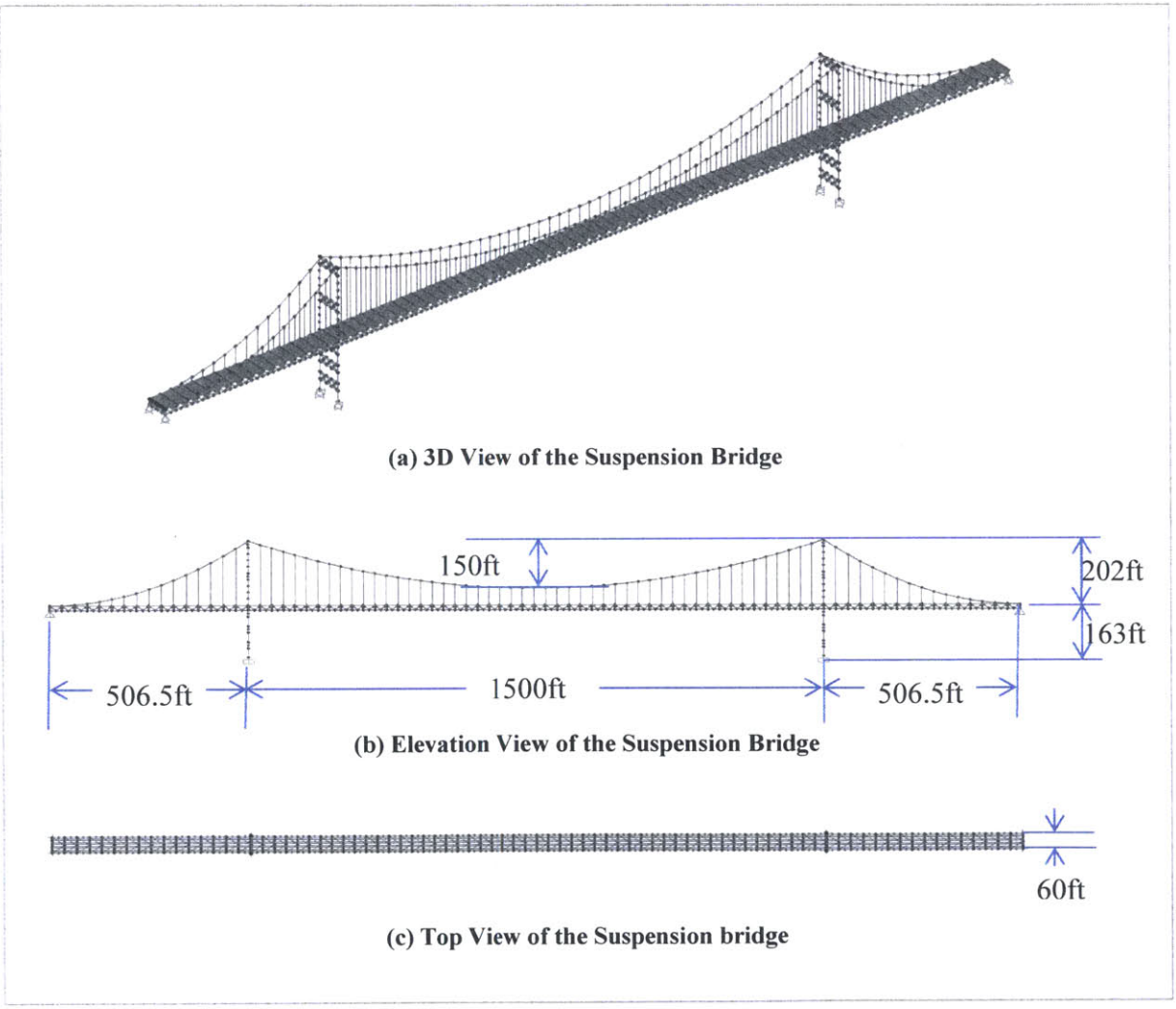

(a) 3D View of the Suspension Bridge

(b) Elevation View of the Suspension Bridge

(c) Top View of the Suspension bridge

Figure 15 Suspension Bridge Model (a) 3D View; (b) Elevation View; (c) Top View

❖ Deck

The width of the suspension bridge deck is 60 feet, which can hold up to four vehicle lanes. Figure 16 describes the deck system using a detailed drawing.

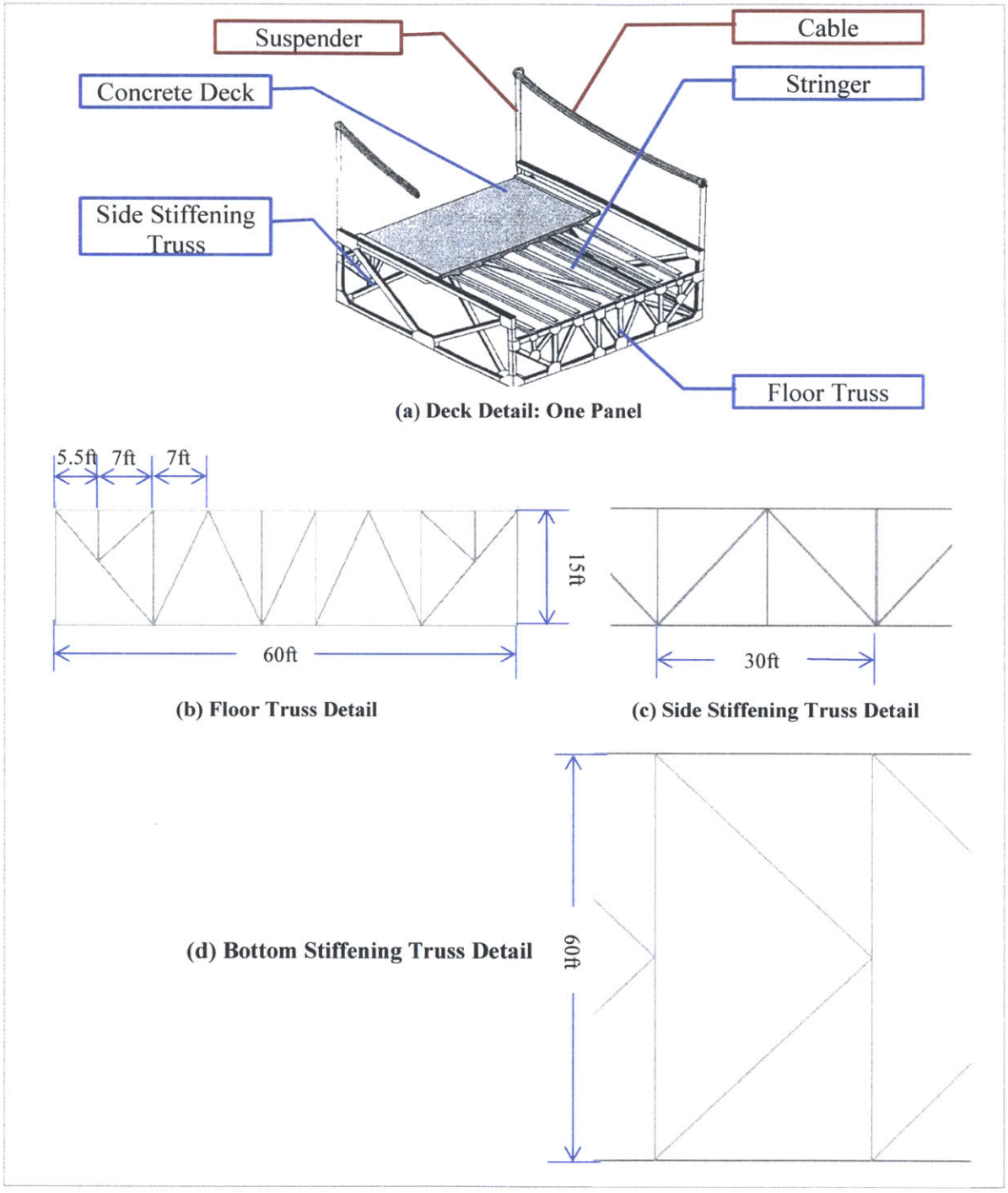

Figure 16 Details of the Deck System

As shown in Figure 16 (a), the concrete deck is spanned over the stringers, which are 7ft apart. The stringers are supported by the floor trusses. A typical floor truss is shown in Figure 16(b). The floor trusses are spread out at 30ft spacing along the longitudinal direction of the bridge, spanning across two stiffening trusses located on both sides of the bridge. The typical configuration of the stiffening trusses is shown in Figure 16 (c). The stiffening trusses are picked up by the hangers at the joints. Then all the loadings are transferred to the main cables, and finally to the towers and anchorages at ends. Additional K truss, described in Figure 16 (d), is placed at the bottom of the deck to increase the bridge's torsional stiffness. The sections of the structural elements that the deck is composed of are listed in Table 1.

Table 1 Deck Element Section

Structural Element		Section
Side Stiffening Truss	Top & Bottom Chord	W12 X 190
	Vertical Member	W12 X 40
	Diagonal Member	W12 x 58
Floor Truss	Intermediate Member	W12 x 40
Bottom Stiffening Truss	Diagonal Member	W10x68
Concrete Deck		0.5ft Thickness

In the SAP model, the concrete deck is modeled as layered shell elements with steel reinforcement bars. All the steel elements of the deck trusses are modeled as frame structure, because the connections between the members, and the connections with the concrete deck provide moment restraints although the members are designed as truss.

❖ Cables & hangers

The main cables are galvanized wire of 1.04ft diameter. The hangers are made of smaller diameters, high-strength wire rope. Both elements are modeled as tendon element in SAP2000, with properties shown in Table 2. In the model, bending moments are released at both ends, while torsional moment is released at the end point of the member.

Table 2 Material Properties of Cable System

Structure Element	Diameter (ft)	Area (ft^2)	F_y (Kip/ft^2)	F_u (Kip/ft^2)	SSCurveOpt
Suspender	1.04	0.817	13575.53	16708.35	250 ksi
Cable	0.2	0.157	26733.35	38638.05	250 ksi

❖ Tower

The suspension bridge has two steel towers. Each tower consists of two steel legs and stiffening truss spanning in between. The total tower height is 365ft, with 202 ft above the deck. Lateral stiffness of the tower is provided by the five trusses spanning between the towers. The configuration of the tower is shown in Figure 17(a). The steel section of the tower legs is shown in Figure 17(b). The truss structure inside the tower is of size W30 x 261.

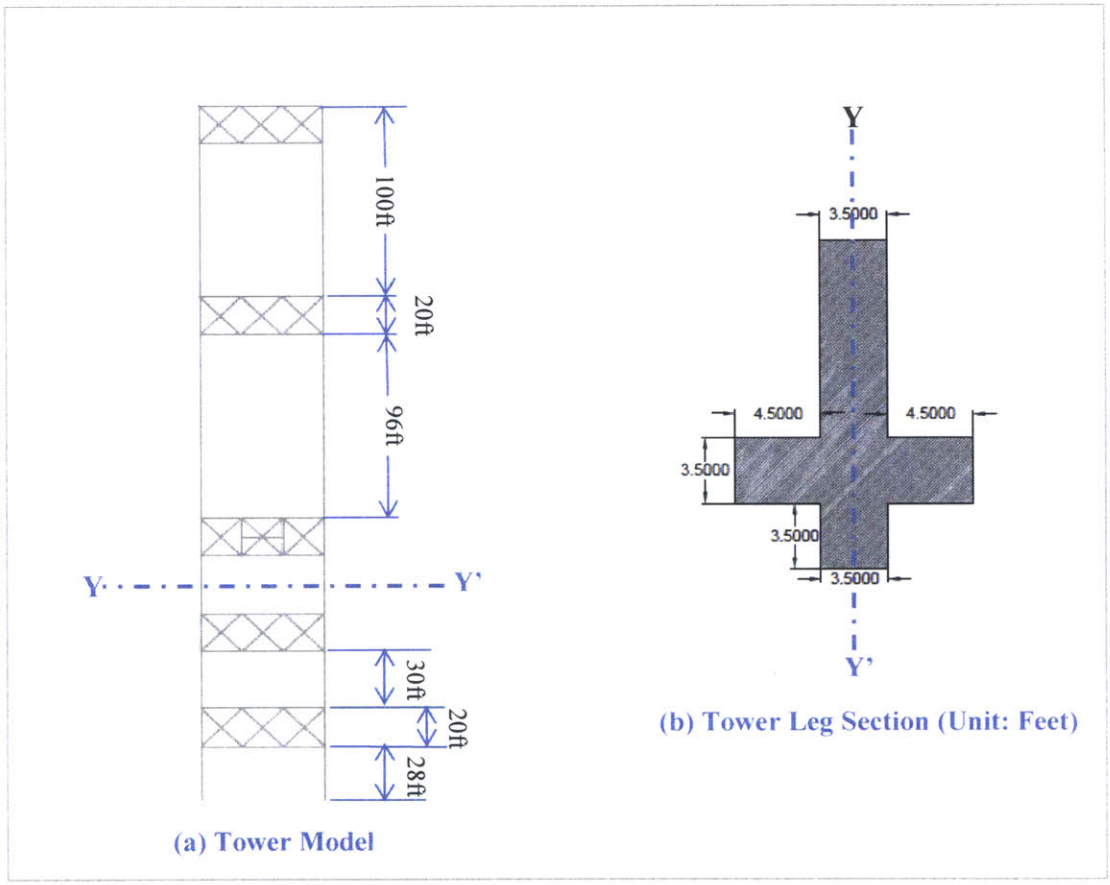

Figure 17 Details of Tower

4.2 Dead Load Analysis

The dead load applied on the structure accounts not only for the self-weight of the structure, but also the appurtenances and attached utilities.

The total dead load applied on the Vincent Thomas Bridge is 7.2kip/ft, which equivalent to 0.12 kip/ft^2 (Shinozuka, 2009). In the SAP model, the dead load is uniformly applied onto the concrete slab elements. The analysis of the static load is important in the suspension bridge, since the cables and suspenders gain stiffness only when they are in tension.

Tension forces in the cables and hangers along the bridge after applying the dead load are shown in Figure 18 and 19.

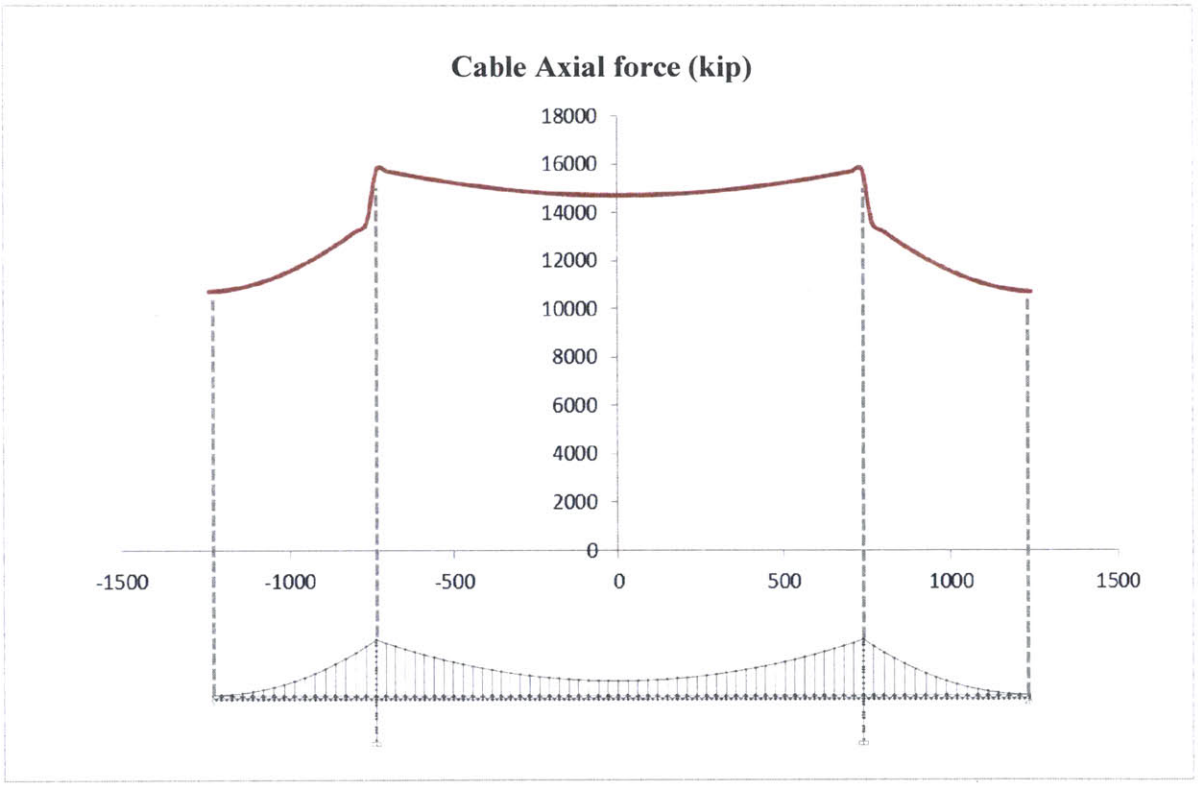

Figure 18 Cable Forces under Dead Load

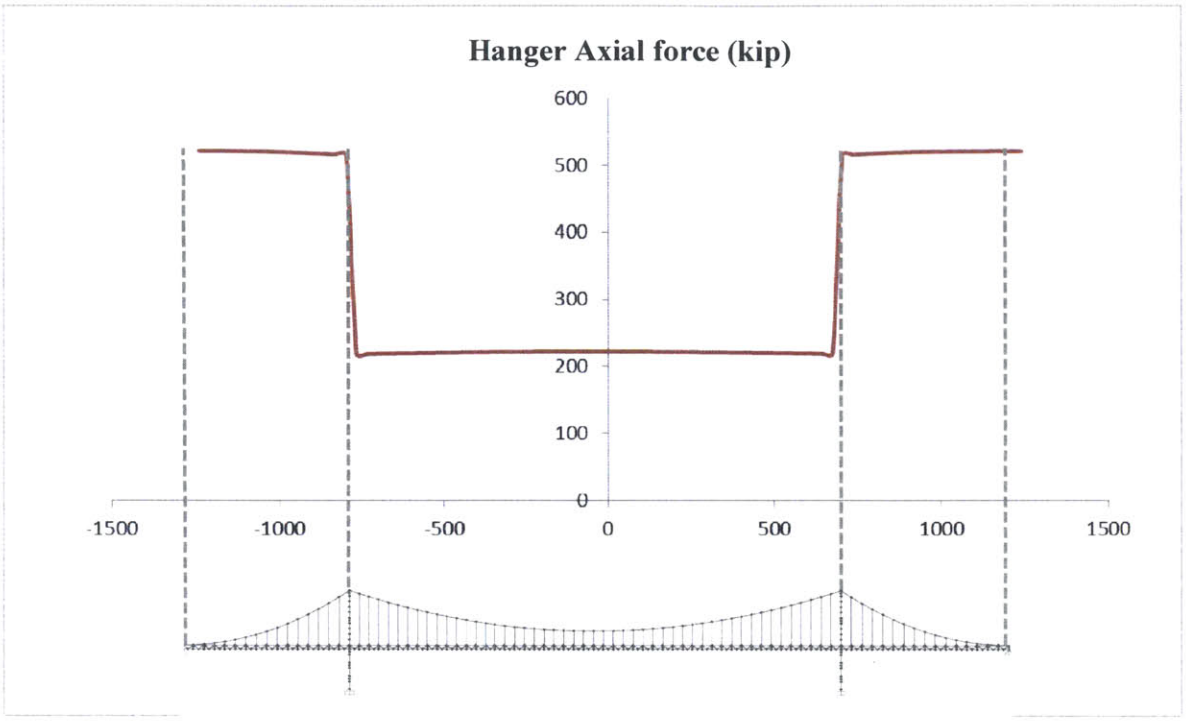

Figure 19 Hanger Cable Forces under Dead Load

4.3 Modal Analysis

Then the calculated tension in the cables and suspenders are assigned to the members with P-Δ force as pre-stressed. Thus, the cable elements can gain stiffness in the modal analysis.

Table 3 shows the first ten modes of the suspension bridge.

Table 3 Modes of the Suspension Bridge

Mode	Modal Shape	Period T (S)	Frequency f(Hz)	Angular frequency ω (rad/s)
1	V-S	9.08	0.1102	0.6922
2	L-S	9.00	0.1111	0.6981
3	L-AS	8.84	0.1131	0.7105
4	V-AS	8.11	0.1232	0.7743
5	T-AS	5.60	0.1787	1.1225
6	L-S	4.97	0.2013	1.2650
7	L-S	4.73	0.2116	1.3295
8	T-S	4.35	0.2300	1.4450
9	V-AS	3.37	0.2968	1.8648
10	V-S	2.63	0.3807	2.3919
Note	L: Lateral		S: Symmetrical	
	V: Vertical		AS: Asymmetrical	
	T: Torsional		V: Vertical	

In this thesis, the focus is on the vertical motion of the bridge, because of two reasons:

- Simplification:
  The focus can simplify analysis of wind load, bridge model and energy harvesting device (SDOF)
- Prevailing failure:
  The simplification is valid in the way that the vertical vibration of the suspension bridge is the major vibration mode that needs to be considered in the design.

Figure 20 shows the first four vertical vibration modal shapes.

(a) Mode 1, T=9.08s

(b) Mode 4, T=8.11s

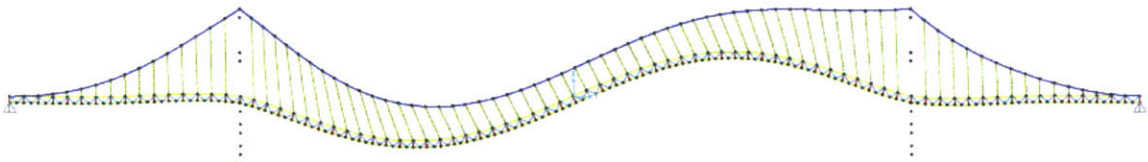

(c) Mode 9, T=3.37s

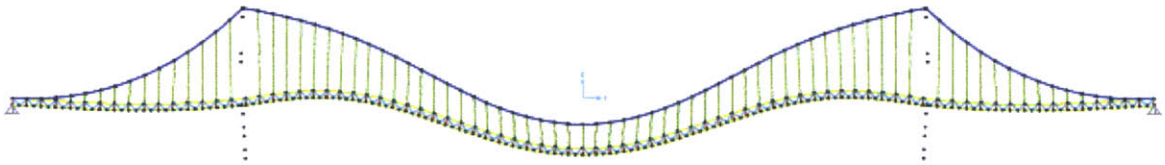

(c) Mode 10, T=2.63s

Figure 20 Vertical Vibration Modes

4.4 Wind Excitation

Wind usually has a relatively smaller frequency and longer period, as shown in Figure 21. When analyzing the suspension bridge under wind vibration, the frequency of the wind that will most likely occur and will have the greatest impact on the structure is the frequency of the first mode.

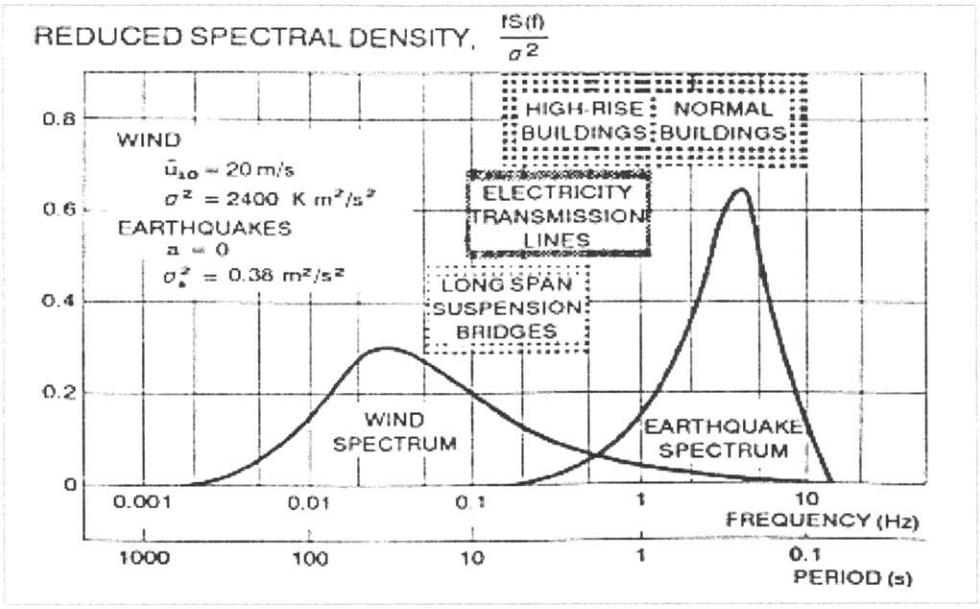

Figure 21 Frequency Features of Wind, Earthquakes and Various Structures

(NatHaz Modeling Laboratory, University of Notre Dame)

According to the sensor recorded data (Shinozuka, 2009), the mean wind speed of the area is 10m/s. The characteristics of the local wind are stated in Table 4.

Table 4 Wind Characteristics

	Mean wind Speed (m/s)	Wind speed time function (m/s)
Horizontal wind	$\bar{U} = 10m/s$	$u(t) = 4\cos(\omega t)$
Vertical Wind	$\bar{W} = 0.25m/s$	$w(t) = 0.1\cos(\omega t)$

❖ Buffeting Force:

Since the motion in the vertical direction of the deck is the main interest, only the forces acting in the vertical direction are accounted for. Referring back to Equation (2.3.20) and substituting all the coefficients as presented in Table 4, the equation can be simplified to

$$L_b(t) = \frac{1}{2}\rho\bar{U}^2 B\left\{\left[\frac{dC_L(0)}{d\alpha} + C_D(0)\right]\frac{w(t)}{\bar{U}}\right\} = \frac{1}{2}\rho\bar{U}B\left[\frac{dC_L(0)}{d\alpha} + C_D(0)\right]w(t) \quad \text{4.4. 1}$$

(Unit: Force per Meter)

Furthermore substituting $\rho, \bar{U}, B, w(t)$ into the Equation (4.4.1), it becomes

$$L_b(t) = 173 \times w(t) = 17.3\cos(\omega t) \quad \text{(Unit: N/m)} \quad \text{4.4. 2}$$

Table 5 Coefficient of the Buffeting Wind Force

Coefficient	Value	Coefficient	Value
C_L	0	C_L'	1.415
C_M	0	C_M'	0.238
C_D	0.162	C_D'	0

From Equation (4.4.1), $L_b(t)$ is proportional to $[\bar{U} \times w(t)]$. Considering w(t) is the vertical component of the wind, w(t) can be seen to be proportional to $[\bar{U}]$. That is saying vertical wind fluctuation force increases with the mean wind speed and is proportional to $[\bar{U}^2]$.

❖ Flutter Force:

Equation (2.3.14) states the calculation of the lift force due to flutter effect. Assuming zero rotation induced by the wind, which is $\dot{\alpha} = \alpha = 0$. The equation is simplified to

$$L_{se}(t) = \frac{1}{2}\rho\bar{U}^2 B\left[KH_1^*\frac{\dot{h}}{\bar{U}}\right] = \frac{1}{2}\rho\bar{U}B\left[KH_1^*\dot{h}\right] \quad \text{4.4. 3}$$

(Unit: Force per unit Length)

Table 6 shows the parameters needed for the calculation of the flutter effect. Substituting the parameters, the force can be represented by

$$L_{se}(t) = 278 \times \dot{h} \quad \text{4.4. 4}$$

Since the wind is fluctuating with the first mode period, the vertical displacement of the bridge deck should be in line with the first vibration mode (with no damping).

$$h = \hat{h}\cos(\omega t) \qquad \text{4.4. 5}$$
$$\dot{h} = -\omega\hat{h}\sin(\omega t)$$

Thus

$$L_{se}(t) = 278 \times \dot{h} = 278 \times \left[-\omega\hat{h}\sin(\omega t)\right] = -192\hat{h}\sin(\omega t) \qquad \text{4.4. 6}$$
(Unit: N/m)

Table 6 Parameter for Flutter Force Calculation

Parameters		Value	Unit
ρ	Air Density	1.2	kg/m3
U	Mean Wind Velocity	10	m/s
B	full width of the Bridge Deck	18.3	m
fi	Modal frequency	0.110	Hz
ω	circular frequency of bridge motion	0.692	rad/s
K	reduced frequency	1.266	s^{-1}
H1*	aerodynamic coefficient	2	
h	vertical wind velocity fluctuation		

The value of $\hat{h}$ can be approximated from the displacement resulted from the buffeting force above. Figure 22 shows the wind fluttering force acting along the bridge.

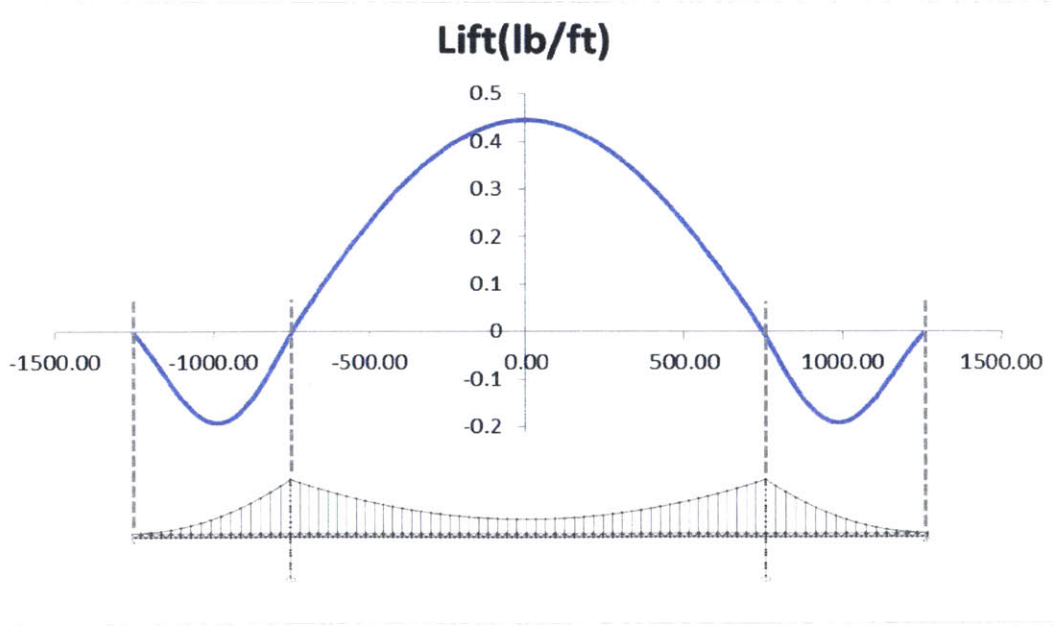

Figure 22 Flutter Wind Force Along the Bridge Deck

4.5 Wind Excitation Response

In the model, apply total lifting force, referring back to equation (4.4.2) and (4.4.6)

$$L(t) = L_{se}(t) + L_b(t) \quad \textbf{4.5.1}$$
$$L_{se}(t) = -192\hat{h}\sin(\omega t) \quad \textbf{4.5.2}$$
$$L_b(t) = 17.3\cos(\omega t) \quad \textbf{4.5.3}$$

The response of the structure can be analyzed for the buffeting effect and fluttering effect separately. Ignoring the damping effect, the vertical displacement of a point on the suspension bridge can be written as:

$$v(t) = v_{se}(t) + v_b(t) \quad \textbf{4.5.4}$$
$$v_{se}(t) = -\hat{v}_{se}\sin(\omega t) \quad \textbf{4.5.5}$$
$$v_b(t) = \hat{v}_b\cos(\omega t) \quad \textbf{4.5.6}$$

Thus

$$v(t) = -\hat{v}_{se}\sin(\omega t) + \hat{v}_b\cos(\omega t) \quad \textbf{4.5.7}$$

Using trigonometric relationship,

$$v(t) = \sqrt{v_{se}^2 + v_b^2}[\cos(\omega t - \varphi)] \quad \textbf{4.5.8}$$
$$tan\varphi = \frac{v_{se}}{v_b} \quad \textbf{4.5.9}$$

Figure 23 plots the structure response amplitudes under the wind loading stated above. Excited by its fundamental modal frequency, the structure experienced maximum vibration at mid-span with amplitude of 0.1125ft. From the graph, the response from the buffeting lifting force dominates the structural response under low wind speed ($\bar{U} = 10m/s$). Thus, the assumption of using response of buffeting force to calculate the fluttering force is valid.

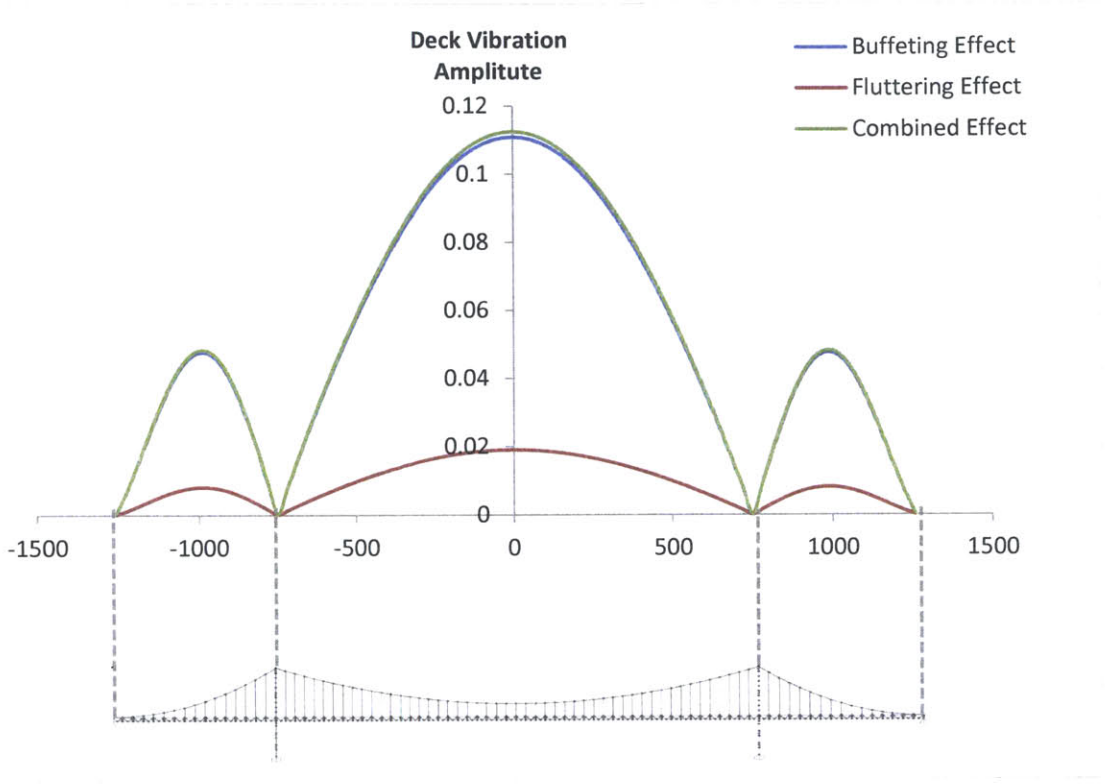

Figure 23 Vibration Amplitude due to Buffeting and Fluttering Effect

As the wind speed changes, the forces exerted on the suspension bridge and the amplitude of vibration change. Figure 24 shows such a change with an increase in the wind speed, where $U_0 = 10m/s$. Response from buffeting effect is in proportion with $(\frac{U}{U_0})^2$, while fluttering effect grows much faster with increase of wind force. When wind speed is large enough, fluttering effect dominates.

As the fluttering effect increases, the assumption that calculation of the fluttering force based on buffeting structural response no longer holds.

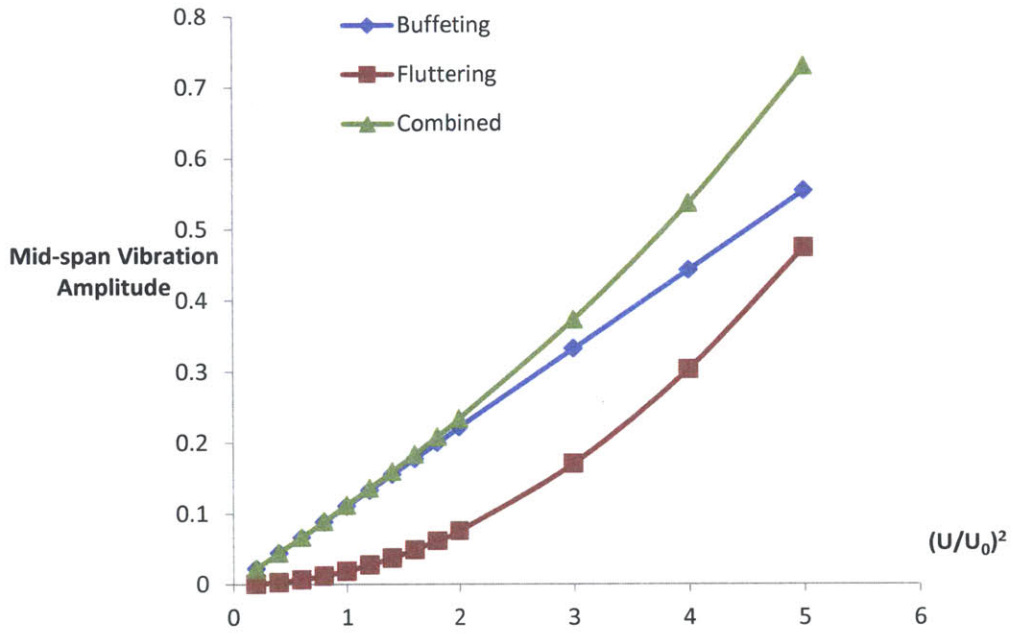

Figure 24 Fluttering and Buffeting Effect on the Structure

4.6 Stiffness of the bridge

If each concrete panel (30ft in length) is treated as an element, the mass for every panel is 98,000kg.

$$m_i = (30ft) \times (7.2\ kip/ft) = 216kip = 97{,}976kg$$

For each element, the equation of motion can be stated as (without damping):

$$m_i \ddot{v}_i + k_i v_i = p$$

Based on the SAP2000 wind buffeting oscillation analysis,

$$p = L_b(t)$$
$$\ddot{v}_i = -\omega^2 v_i$$

Then the stiffness k_i can be calculated as

$$k_i = \frac{L_b(t)}{v_i} + m\omega^2$$

The calculated k_i along the bridge is shown in Figure 25. The stiffness at the support of the bridge is largest.

Later in section 5.4, energy harvesting devices are implemented at the center part of the middle span, and an average stiffness k_{ave} is considered. Refer to the red line indicated in Figure 25.

$$k_{ave} = 127{,}000N/m$$

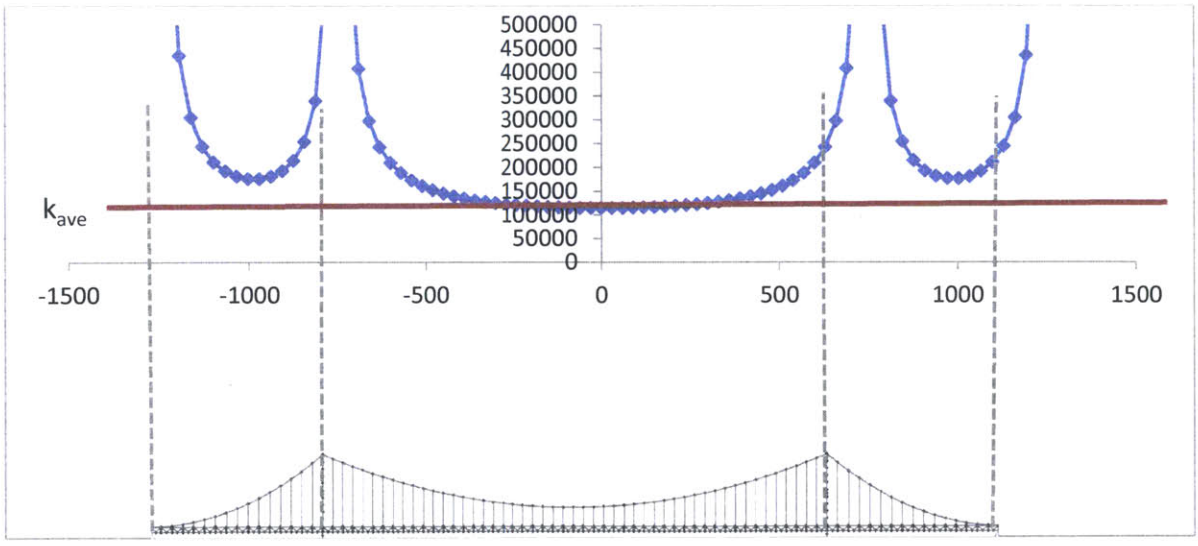

Figure 25 Stiffness along the Bridge (the Red Line Indicates the Average Stiffness Position)

Chapter 5 Feasibility Study of Energy Harvesting Device

5.1 Introduction

The electromagnetic energy harvesting devices are proposed to be placed along the suspension bridge to harvest energy. The idea of having electromagnetic energy harvesting devices is that, with the right design, the mass resonant part of the device can amplify the vibration of the main structure within a limited magnetic field. Moreover, with the increase of the mass of the device, it can result in the structure acting as a tuned mass damper to control the motion of the structure.

Since the fundamental vibration mode of the bridge has a low frequency of 0.11Hz, which is out of the range of most developed energy harvesters, a new device with low stiffness (k/m) value needs to be established. In section 5.2, a simple linear resonant (LR) Energy harvesting device with low resonant frequency was sketched, and the potential energy that could be harvested was calculated in terms of power.

Then in section 5.3, nonlinearity is introduced into the LR device, to increase the bandwidth of energy that could be harvested. However, with introducing the nonlinearity, the natural frequency of the device cannot be reduced to the desired value.

In section 5.4, an array of energy harvesting device is designed as tuned mass damper for each concrete slab of the bridge with equivalent mass, and damping ratio. The potential energy that can be harvested was displayed as well.

5.2 Simple Linear Resonant (LR) Energy Harvester

Figure 26 shows a simple Electromagnetic Energy Harvesting device, with two identical magnets repulsing each other, a spring attach to the upper magnet and coil. The purpose of the spring is to adjust the stiffness of the system to achieve target value and to allow the mass to move up and down.

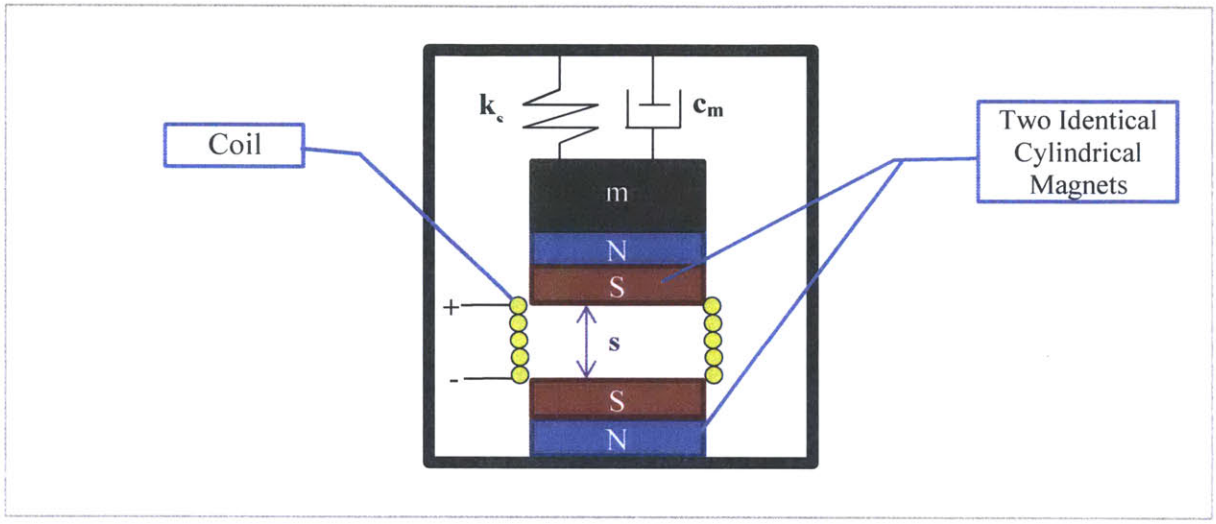

Figure 26 A Simple LR Energy Harvester

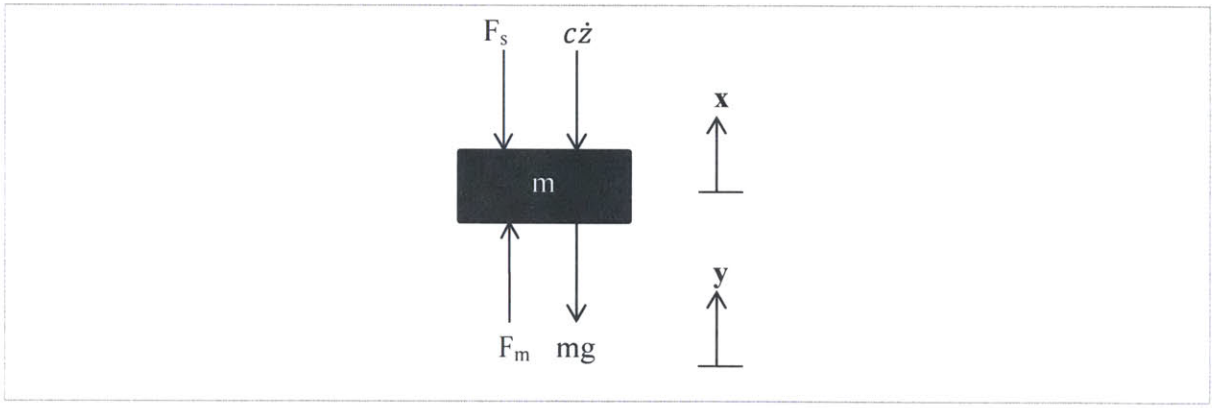

Figure 27 Modeled Mass Damper System

First, the device was simplified as a mass damper system, as shown in Figure 27. Since the single mass is very small compared to the structure it's attached to, it has little impact on the structure. The equation of motion can be written as:

$$m\ddot{x} + c\dot{x} + F_s + mg = F_m - m\ddot{y} \qquad \textbf{5.2. 1}$$

Then it can simplified

$$m\ddot{z} + c\dot{z} + k_{eq}z = -m\ddot{y} \quad \text{5.2. 2}$$

Where,

y: Host structure displacement;

x: Mass displacement;

$z = x - y$: relative displacement between the mass and the host structure;

k_{eq}: Equivalent stiffness;

$c = c_e + c_m$: Total damping effect. Since the transfer of energy to electrical energy is through electromagnetic induction, which is related to the speed of the mass damper ($\dot{x}$), the energy transferred can be represented by damping (c_e), while the mechanical damping like friction is represented by c_m;

s: spacing between the two magnets;

F_m(s): Magnetic force on the mass, which is a function of spacing s;

F_s: Spring force on the mass;

The most efficient mass damper is the one with natural frequency equals to the excitation frequency. If a mass of $m = 2kg$ is used here, the equivalent stiffness can be calculated as:

$$k_{eq} = m\omega^2 = (2)(0.69) = 1.38 \text{ (Unit: N/m)} \quad \text{5.2. 3}$$

Denoteing

s_e: Spacing between the two magnets under static equilibrium state;

F_{se}: Spring force on the mass at static equilibrium;

In the static equilibrium state, the equilibrium equation can be written as

$$F_m(s_e) = F_{se} + mg \quad \text{5.2. 4}$$

Combined with equation (5.2.2):

$$k_{eq}z = kx + F_{m_{se}} + mg - F(s_e + z) = kx + F_m(s_e) - F_m(s_e + z) \quad \text{5.2. 5}$$

Applying linearization theory:

$$F_m(s_e) - F_m(s_e + z) = F'(s_e)z \quad \text{5.2. 6}$$

Thus,

$$k_{eq} = k - F'_m(s_e) \quad \text{5.2. 7}$$

Magnetic force between the two identical cylindrical structures is presented in equation (2.2.1)

$$F(s) = \frac{\pi B_0^2}{\mu_0} R^4 [\frac{1}{s^2} + \frac{1}{(s+2h)^2} - \frac{2}{(s+h)^2}] \quad \text{5.2. 8}$$

The derivative of the Equation (5.2.8) with respect to s:

$$F'(s) = -2 \times \frac{\pi B_0^2}{\mu_0} R^4 [\frac{1}{s^3} + \frac{1}{(s+2h)^3} - \frac{2}{(s+h)^3}] \quad \text{5.2. 9}$$

For the practical study, the magnet used is shown in Figure 27, and the properties of the magnet are listed in table 6.

Figure 28 Ferrite Disc Magnet (FE-S-40-20 Supermagnete)

Table 7 Properties of the ferrite disc magnet

		Value	Unit
R	Radius	0.02	m
h	Height	0.02	m
ϱ	Density	4800	kg/m^3
m	Mass	0.120637158	kg
B_0		0.4	T
μ_0		1.25664E-06	N A−2

Studying the equilibrium equation (5.1.7), with varying distances between the two magnets, we can have a range of spring stiffness k_s that can be chosen, as shown in Figure 29. The equilibrium spacing of two magnets is important, since it determines the number of turns of the coil.

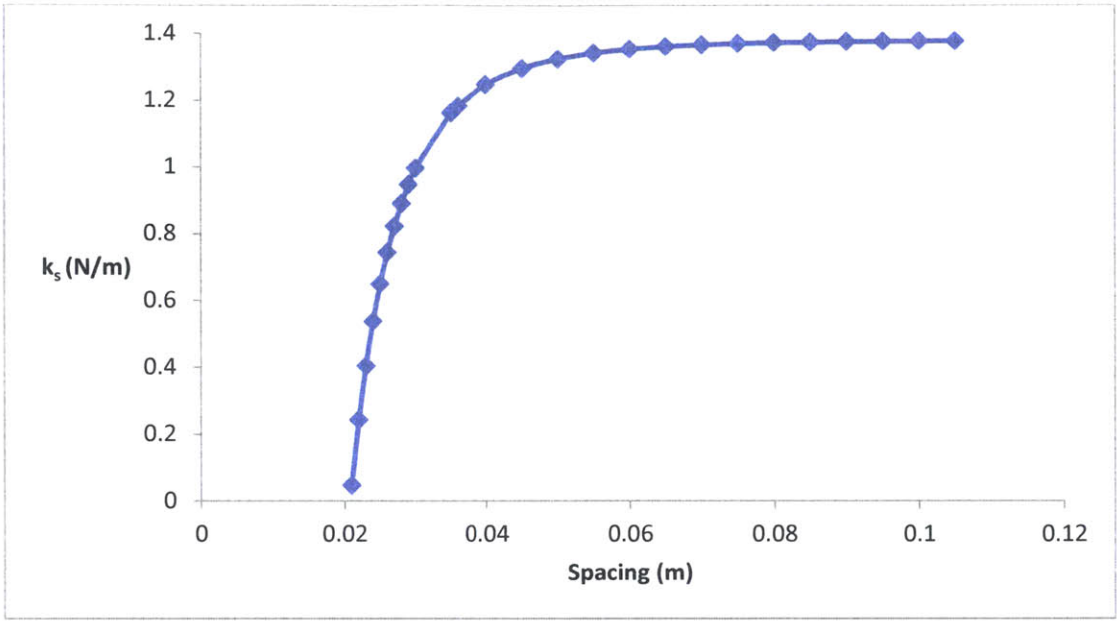

Figure 29 Required Spring Stiffness Varying with Spacing between the Magnets

The equilibrium elongation of the spring is also important, to determine the size of the device. The relationship between the elongation and the spacing is shown in Figure 30. If choosing an equilibrium spacing of 0.036m, a reasonable static equilibrium elongation of the spring of 0.0226 m can be achieved.

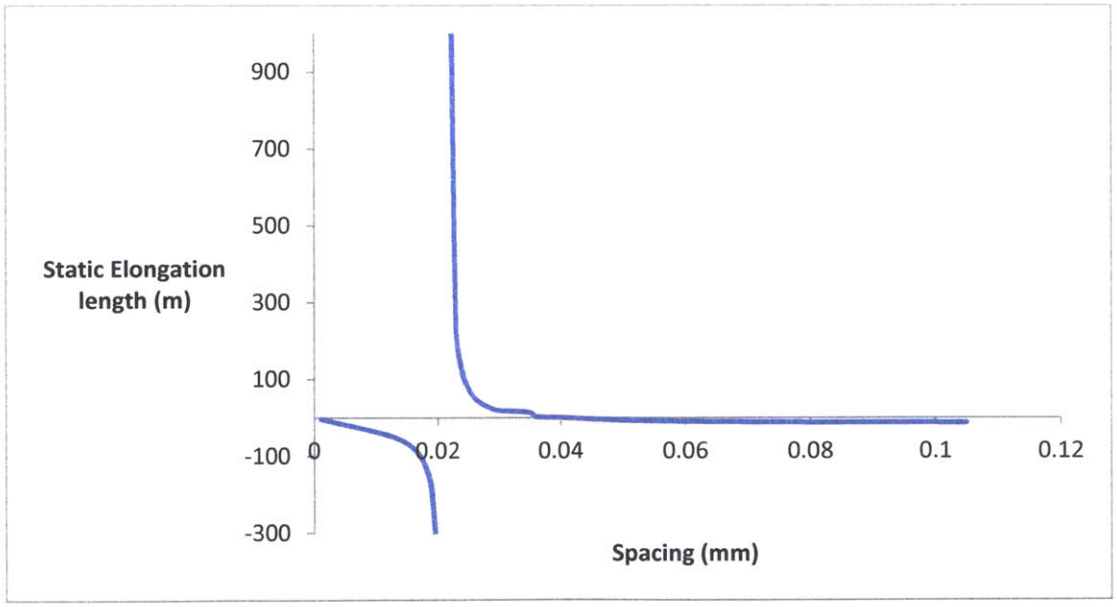

Figure 30 Spring Equilibrium Elongation (L_{se}) Varying with Spacing between Two Magnets

The coil in the device is made of copper, and its properties are listed in Table 8.

Table 8 Copper Coil Property

Copper Coil Property	Value	Unit
diameter	2.588	mm
Turns of wire	3.86	turns/cm
Resistance	3.277	mΩ/m

The LR energy harvesting device properties are listed in Table 9.

Table 9 LR Energy harvesting Device properties

Name		Value	Unit
Mass	m	2	kg
Angular Frequency	ω	0.831	rad/s
Equilibrium Spacing	S_e	0.1	m
Equilibrium Spring Elongation	L_{se}	0.258	m
Spring Stiffness	k_s	1.183	N/m
Number Of Turns In Coil	N	50	turns
Wire Length Of Coil	l	6.283	Ω
Magnetic Flux	B	0.824	T
Resistance Of Coil	R_c	0.021	Ω
Mechanical Damping	c_m	1	Ns/m
Mechanical Damping Ratio	ζ_m	0.301	Unit less
Load Resistance	R_L	258.95	Ω
Electro- mechanic Damping	c_e	1	Ns/m
Electro-mechanic Damping Ratio	ζ_e	0.301	Unit less
Total Damping Ratio	ζ	0.602	Unit less

Magnetic field strength B is calculated using equation (2.2.1) and (2.2.2).

$$F(s) = \frac{\pi B_0^2}{\mu_0} R^4 \left[\frac{1}{s^2} + \frac{1}{(s+2h)^2} - \frac{2}{(s+h)^2}\right] = \frac{AB(s)^2}{2\mu_0} \qquad \textbf{5.2. 10}$$

Thus, the magnetic field strength as a function of spacing s is illustrated as

$$[B(s)]^2 = \frac{2\pi B_0^2}{A} R^4 \left[\frac{1}{s^2} + \frac{1}{(s+2h)^2} - \frac{2}{(s+h)^2}\right] = 2B_0^2 R^2 \left[\frac{1}{s^2} + \frac{1}{(s+2h)^2} - \frac{2}{(s+h)^2}\right] \qquad \textbf{5.2. 11}$$

Rc is the resistant of the coil.

R_L is can be optimized using equation (2.1.10), so that $c_m = c_e$.

Initially, the mechanical damping c_m is taken as the friction force of the mass as 1Nm/s. It can be adjusted according to usage.

With $\omega = \omega_n$, the mass vibration amplitude (from Equation (2.1.3)) can be expressed as

$$z = \frac{1}{2\zeta} Y sin(\omega t - \varphi) = Z sin(\omega t - \varphi) \qquad \textbf{5.1. 12}$$

Based on the wind oscillation, the vibration of the deck of the suspension bridge is y, the z can be calculated, and it is shown in Figure 31.

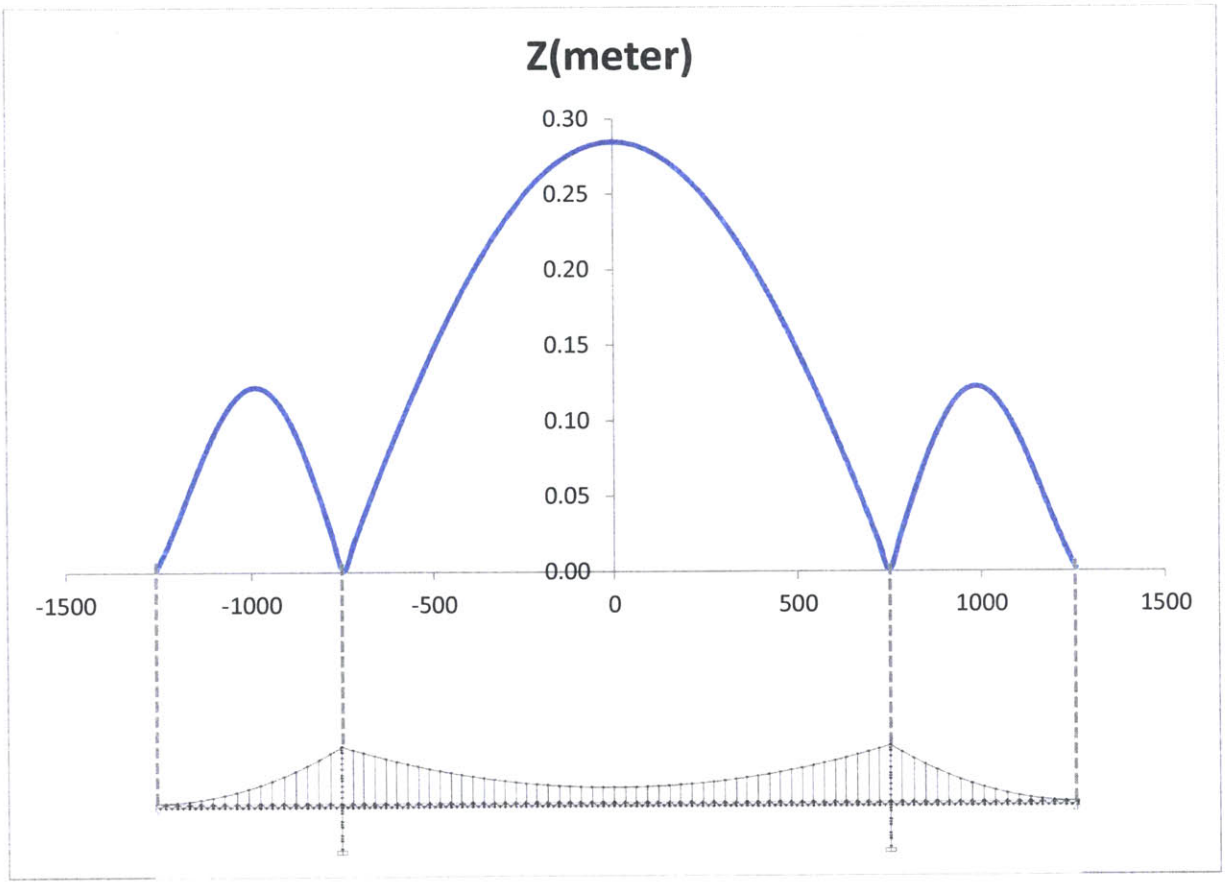

Figure 31 Vibration Amplitude of the Mass of the Energy Harvester Installed along the Bridge

Substituting equation (5.1.12) into equation (2.1.7), the power output of the device can be calculated.

$$P_e = \frac{1}{2} c_e \omega^2 z^2 = \frac{1}{2} c_e \omega^2 (Z)^2 \, [sin^2(\omega t - \varphi)] \qquad \textbf{5.1. 13}$$

$$= \frac{1}{2} c_e \omega^2 (\frac{1}{2\zeta} Y)^2 \, [sin^2(\omega t - \varphi)] = \widehat{P_e} \, [sin^2(\omega t - \varphi)]$$

The potential energy power can be harvested with respect to the location of the energy harvester as shown in Figure 32.

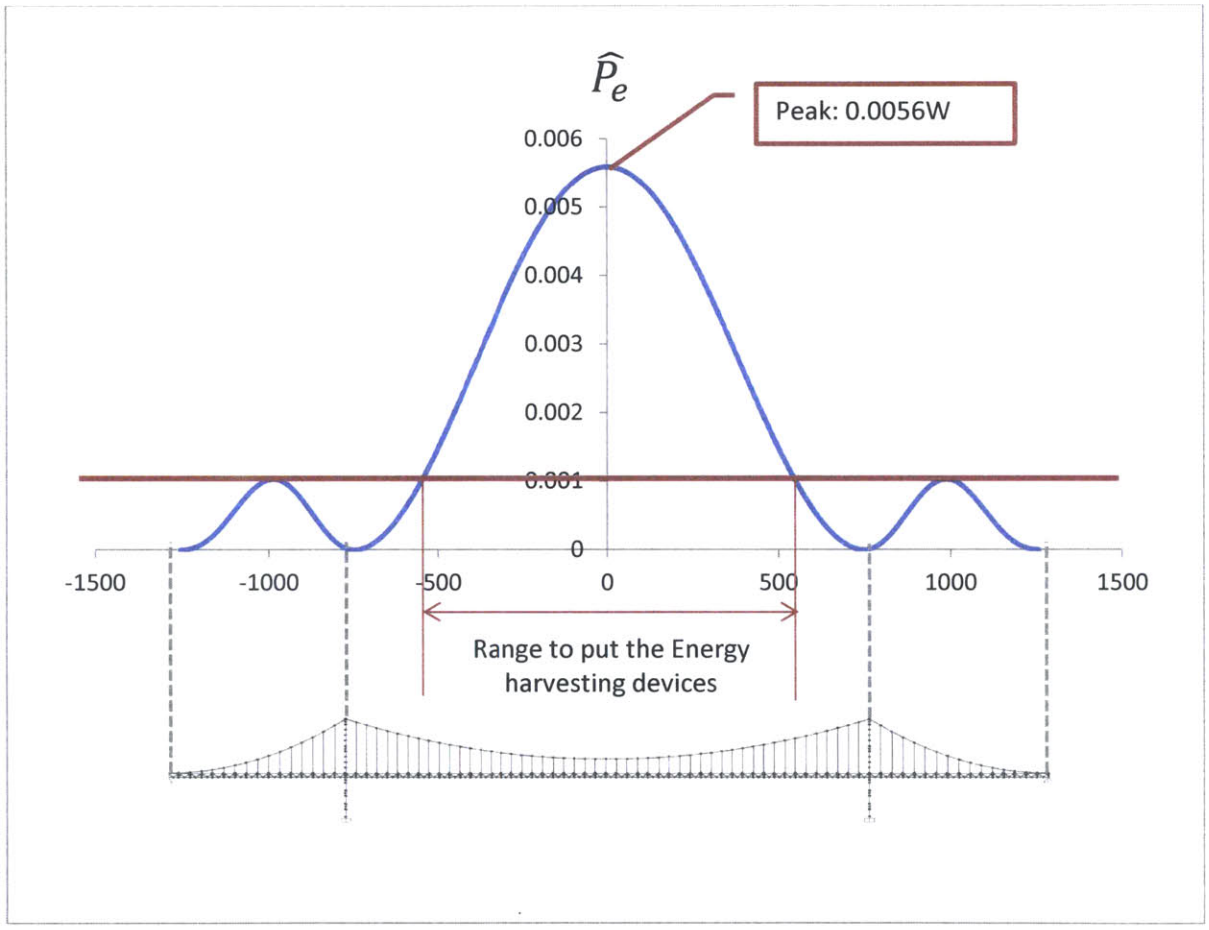

Figure 32 Potential Power Amplitude of the Mass of the Energy Harvester Installed along the Bridge

The energy harvester is placed where the energy output is larger than 0.001W per energy harvester, as shown in Figure 32, above the red line, in the middle of the span. If such a device is placed in the middle of the concrete slab of the bridge, which is 30ft apart, the total energy power $\widehat{P_e} = 0.15W$.

The dimension of such a device is around 40mm in diameter, while the concrete slab is 30ftx60ft. Attaching 50, 100 or even more devices onto the slab increase the power output proportionally.

The mechanical damping can be adjusted to maximize the power output. Since the total power output is proportional to the peak power output. The relationship between peak power output and the value of mechanical damping c_m is depicted in Figure 33. The power output can be maximized by minimizing the mechanical damping.

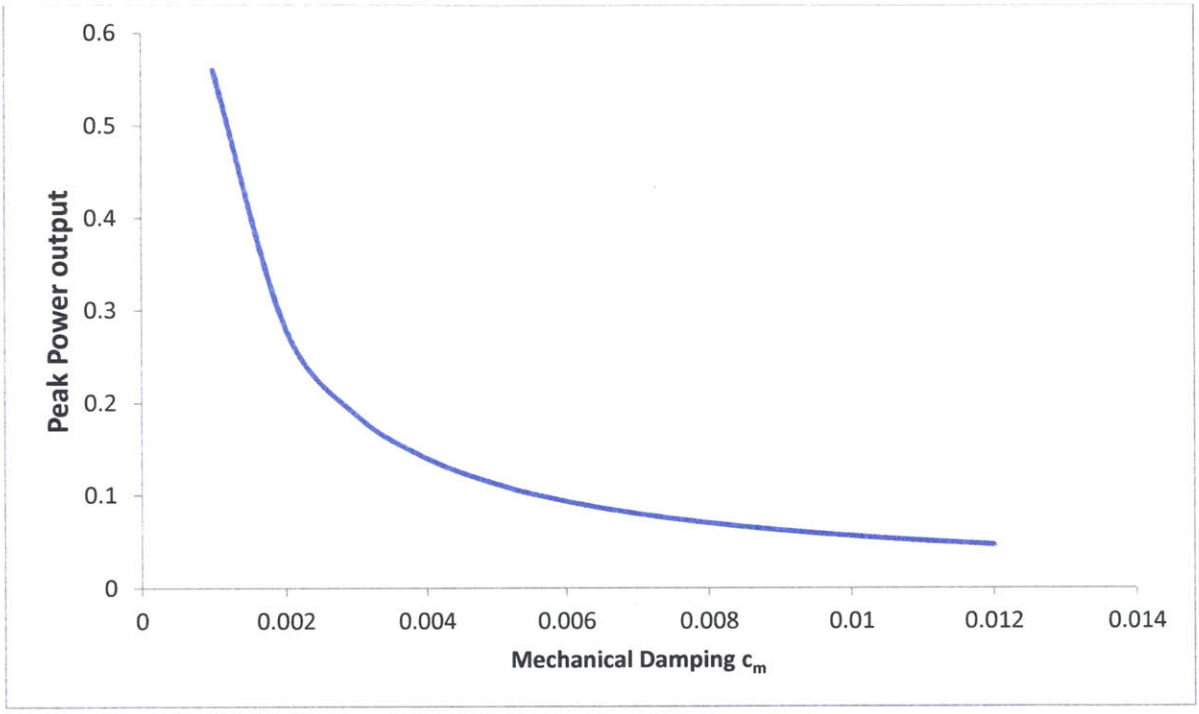

Figure 33 Peak Power Output Varying with Mechanical Damping

5.3 Nonlinear Energy Harvester

Figure 34 illustrates the nonlinear energy harvesting device.

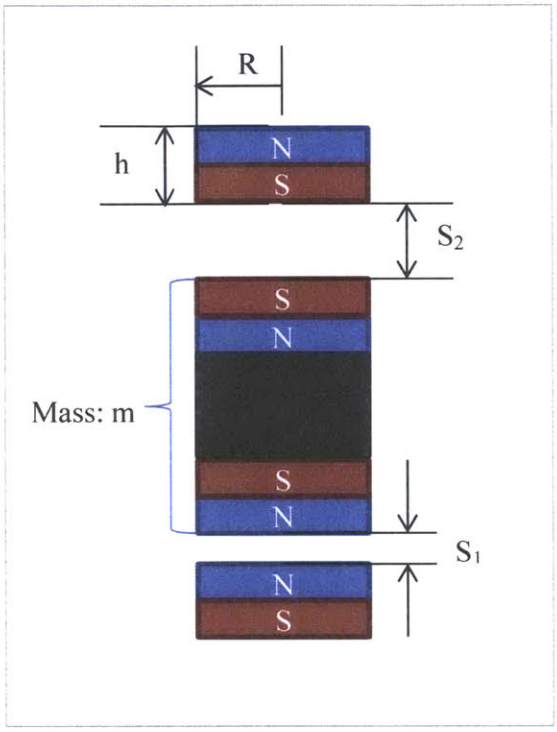

Figure 34 Nonlinear Energy Harvester

The magnetic force in between the lower and upper magnets:

$$F_1(s_1) = \frac{B_0^2\pi}{\mu_0}R^4\left[\frac{1}{{s_1}^2} + \frac{1}{(s_1+2h)^2} - \frac{2}{(s_1+h)^2}\right]$$
$$= \frac{B_0^2\pi}{\mu_0}R^2\left[\frac{1}{(\frac{s_1}{R})^2} + \frac{1}{\left(\frac{s_1}{R}+\frac{2h}{R}\right)^2} - \frac{2}{\left(\frac{s_1}{R}+\frac{h}{R}\right)^2}\right] \quad \textbf{5.3. 1}$$

$$F_2(s_2) = \frac{B_0^2\pi}{\mu_0}R^4\left[\frac{1}{{s_2}^2} + \frac{1}{(s_2+2h)^2} - \frac{2}{(s_2+h)^2}\right]$$
$$= \frac{B_0^2\pi}{\mu_0}R^2\left[\frac{1}{(\frac{s_2}{R})^2} + \frac{1}{\left(\frac{s_2}{R}+\frac{2h}{R}\right)^2} - \frac{2}{\left(\frac{s_2}{R}+\frac{h}{R}\right)^2}\right]$$

Substitute $\alpha_1 = \frac{s_1}{R}, \alpha_2 = \frac{s_2}{R}, \alpha_0 = \frac{h}{R}$ into Equation (5.3.1)

$$F_1(\alpha_1) = \frac{B_0^2\pi}{\mu_0} R^2 \left[\frac{1}{{\alpha_1}^2} + \frac{1}{(\alpha_1 + 2\alpha_0)^2} - \frac{2}{(\alpha_1 + \alpha_0)^2}\right] = \frac{B_0^2\pi}{\mu_0} R^2 f(\alpha_1)$$
$$F_2(\alpha_2) = \frac{B_0^2\pi}{\mu_0} R^2 \left[\frac{1}{{\alpha_2}^2} + \frac{1}{(\alpha_2 + 2\alpha_0)^2} - \frac{2}{(\alpha_2 + \alpha_0)^2}\right] = \frac{B_0^2\pi}{\mu_0} R^2 f(\alpha_2) \quad \textbf{5.3. 2}$$

$f(\alpha_i)$ is a dimensionless function:

$$f(\alpha_i) = \frac{1}{(\frac{s_i}{R})^2} + \frac{1}{\left(\frac{s_i}{R} + \frac{2h}{R}\right)^2} - \frac{2}{\left(\frac{s_i}{R} + \frac{h}{R}\right)^2} \quad \textbf{5.3. 3}$$

Static Equilibrium station:

$$F_1(\alpha_{e1}) - F_2(\alpha_{e2}) = mg \quad \textbf{5.3. 4}$$

Substitute Equation (5.3.2) into Equation (5.3.4)

$$\frac{B_0^2\pi}{\mu_0} R^2 [f(\alpha_{e1}) - f(\alpha_{e2})] = mg \quad \textbf{5.3. 5}$$

With relative movement x,

$$\alpha = \frac{x}{R}$$

$$s_1 = s_{e1} + x \rightarrow \alpha_1 = \alpha_{e1} + \alpha$$
$$s_2 = s_{e2} - x \rightarrow \alpha_2 = \alpha_{e2} - \alpha \quad \textbf{5.3. 6}$$

The motion equation can be written as:

$$m\ddot{x} + F(\alpha_2) + mg - F(\alpha_1) = 0 \quad \textbf{5.3. 7}$$

Substitute Equation (5.3.2), (5.3.5) and (5.3.6) into (5.3.7)

$$m\ddot{x} + \frac{B_0^2\pi}{\mu_0} R^2 \{-[f(\alpha_{e1} + \alpha) - f(\alpha_{e1})] - [f(\alpha_{e2}) - f(\alpha_{e2} - \alpha)]\} = 0 \quad \textbf{5.3. 8}$$

From Taylor expansion, we know that

$$f(\alpha_{e1}+\alpha) = f(\alpha_{e1}) + f'(\alpha_{e1})\alpha + \frac{1}{2}f''(\alpha_{e1})\alpha^2 + \frac{1}{6}f^{(3)}(\alpha_{e1})\alpha^3 + \cdots$$
$$f(\alpha_{e2}-\alpha) = f(\alpha_{e2}) + f'(\alpha_{e2})(-\alpha) + \frac{1}{2}f''(\alpha_{e1})(-\alpha)^2 + \frac{1}{6}f^{(3)}(\alpha_{e1})(-\alpha)^3 + \cdots \quad \textbf{5.3. 9}$$

❖ Linear Analysis

In linear analysis, assuming α is small enough; linear relationship can be established as Equation (5.3.10) when substituting Equation (5.3.9) with α to the first order.

$$m\ddot{x} + \frac{B_0^2\pi}{\mu_0}R^2[-f'(\alpha_{e1}) - f'(\alpha_{e2})]\alpha = 0 \quad \textbf{5.3. 10}$$

With$\alpha = \frac{x}{R}$, stiffness value can be calculated as

$$k = \frac{B_0^2\pi}{\mu_0}R[-f'(\alpha_{e1}) - f'(\alpha_{e2})] \quad \textbf{5.3. 11}$$

❖ Nonlinear Analysis

In nonlinear analysis, Equation (5.1.9) is substituted into Equation (5.1.7) with α to the third order.

$$m\ddot{x} + \frac{B_0^2\pi}{\mu_0}R^2\{[-f'(\alpha_{e1}) - f'(\alpha_{e2})]\alpha + \frac{1}{2}[-f''(\alpha_{e1}) + f''(\alpha_{e2})]\alpha^2 + \frac{1}{6}\left[-f^{(3)}(\alpha_{e1}) - f^{(3)}(\alpha_{e2})\right]\alpha^3 = 0 \quad \textbf{5.3. 12}$$

The term containing α^2 can be ignored, since the coefficient of the term can be cancelled.

The linear and nonlinear coefficient k and k_3 can be calculated as follows

$$k = \frac{B_0^2\pi}{\mu_0}R[-f'(\alpha_{e1}) - f'(\alpha_{e2})]$$
$$k_3 = \frac{B_0^2\pi}{\mu_0}\frac{1}{6R}\left[-f^{(3)}(\alpha_{e1}) - f^{(3)}(\alpha_{e2})\right] \quad \textbf{5.3. 13}$$

Table 10 shows the property of the magnet used in the device for this analysis

Table 10 Ferrite Magnet Properties

FE-S-40-20
Disc magnet Ø 40 mm, height 20 mm, ferrite, Y35, no coating, strength: approx. 4,7 kg

Name		Value	Unit
Radius of magnet	**R**	0.02	m
Height of magnet	**h**	0.02	m
Density	**ϱ**	4800	kg/m^3
Mass	**m**	2	kg
Stiffness (desired)	**k**	1.38	N/m
Magnetic field	**B_r**	0.4	T
Vacuum permitivity	**μ0**	1.25664E-06	N A−2
	M	636619.7724	A/m

Upon calculation, it is found that it is impossible to get k/m to the desired value.

5.4 Equivalent Tuned Mass Damper

The mass damper studied above is relatively small, with a mass of 2kg. The mass is so small compared to the mass of the bridge and thus it has a negligible effect.

An array of devices can be implemented on the bridge, with enough number of devices, it can behave as a tuned mass damper system, and the energy can be harvested simultaneously. The device described in section 5.2 can be implemented onto the structure and placed on the concrete deck.

Referring to the motion based design (Connor, 2002), the original suspension bridge can be seen as undamped structure.

The motion of the undamped structure with the installation of energy harvesting device is described by the equation:

$$\bar{u} = \frac{\hat{p}}{k} H_1 e^{i\delta_1} - \frac{\hat{a}_g m}{k} H_2 e^{i\delta_2} \qquad 5.4.1$$

The motion of the Energy harvester is

$$\bar{u}_d = \frac{\hat{p}}{k} H_3 e^{-i\delta_3} - \frac{\hat{a}_g m}{k} H_4 e^{-i\delta_3} \qquad 5.4.2$$

Two cases are discussed here with equivalent damping of 0.02 and 0.04.

5.4.1. $\zeta_{eq} = 0.02$

Table 11 Equivalent Mass Damper with Damping Ratio of 0.02

Notation	Value	Unit
ζe	0.02	Unit less
H2-opt	25	Unit less
$\bar{m}$	0.0003	Unit less
fopt	1	Unit less
m_i	98,000	kg
md	30	kg
ζd-opt	0.0035	Unit less
k_{ave}	127000	N/m

Table 11 can be interpreted as: if the energy harvesters are installed to control the motion of the bridge concrete panel, each concrete panel needs a total of fifteen such devices. Moreover, the

fifteen devices acting together will have an equivalent damping ratio of 0.35%. Thus, each device should have a damping ratio of $0.35\% \div 15 = 0.023\%$.

To achieve the required damping ratio, the c_m value of each device used can be adjusted. Table 12 shows the parameters of the adjusted energy harvesting device.

Table 12 Required Energy Harvesting Device Coefficients (0.02 damping)

		Value	Unit
mass	m	2.000	kg
Resistance of coil	R_{coil}	0.021	Ω
Mechanical	c_m	0.00038	Ns/m
mechanical Damping Ratio	ζ_m	0.0115%	unit less
Load Resistance	R load	43155.623	Ω
Electro-mechanic damping	c_e	0.00038	Ns/m
Electro-mechanic damping ratio	ζ_e	0.0115%	unit less
total damping ratio	ζ	0.0036	unit less

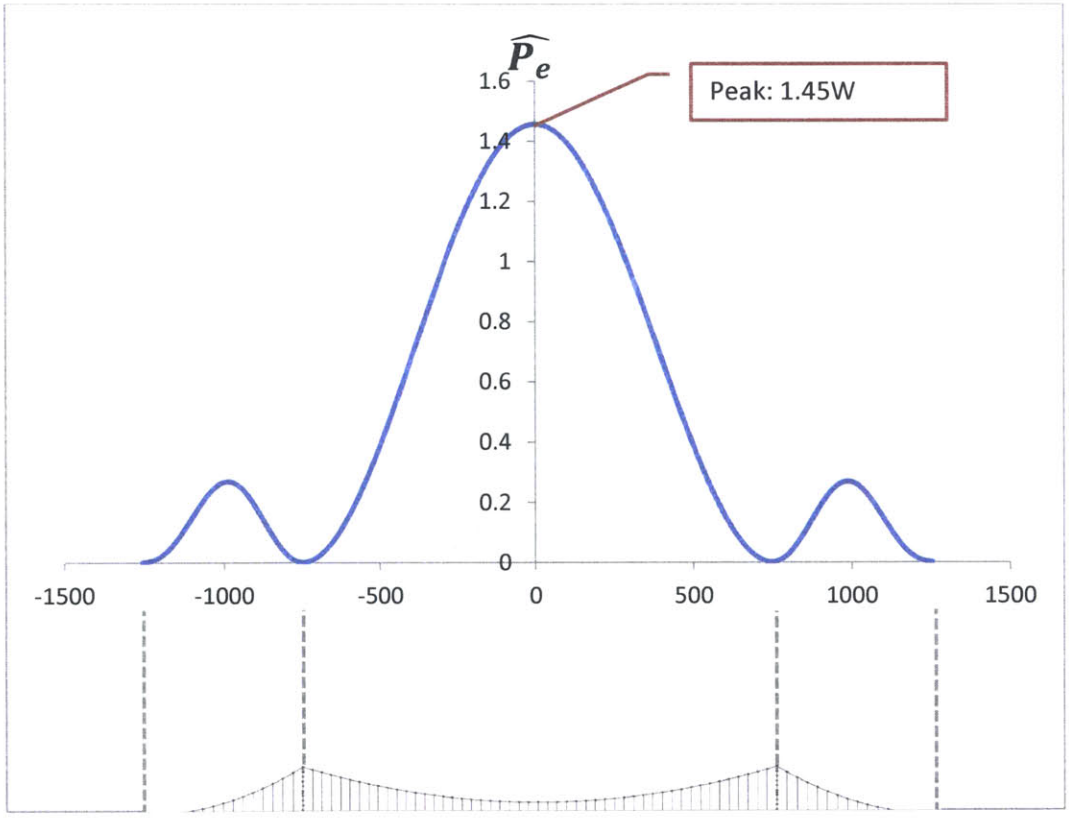

Figure 35 Potential Power Amplitude of the Mass of the Energy Harvester Installed along the Bridge for Equivalent Damping Equal to 0.02

The total energy with 15 devices per pannel is calculated to be 616W.

5.4.2. $\zeta_{eq} = 0.04$

Table 13 Equivalent Mass Damper with Damping Ratio of 0.04

Notation	Value	Unit
ζe	0.04	Unit less
H2-opt	12.5	Unit less
$\bar{m}$	0.015	Unit less
fopt	0.982	Unit less
m_i	98,000	kg
md	1470	kg
ζd-opt	0.075	Unit less
k_{ave}	127,000	N/m

Table 13 can be interpreted as: if the energy harvesters are installed to control the motion of the bridge concrete panel, each concrete panel need 735 such devices. Furthermore, 735 devices acting together will have an equivalent damping ratio of 7.5%. Therefore, each device should have a damping ratio of $7.5\% \div 735 = 0.01\%$.

Again, c_m value can be adjusted to reach the damping ratio requirement. Table 14 shows the parameters of the adjusted energy harvesting device.

Table 14 Required Energy Harvesting Device Coefficients (0.02 damping)

		Value	Unit
Mass	m	2.000	kg
Resistance of coil	R_{coil}	0.021	Ω
Mechanical damping	c_m	0.00018	Ns/m
mechanical Damping Ratio	ζ_m	0.00005	unit less
Load Resistance	R load	20.6	Ω
Electro-mechanic damping	ce	0.00018	Ns/m
Electro-mechanic damping ratio	ζe	0.00005	unit less
total damping ratio	ζ	0.0001	unit less

The total energy with 735 devices per pannel is calculated to be 75.7kW.

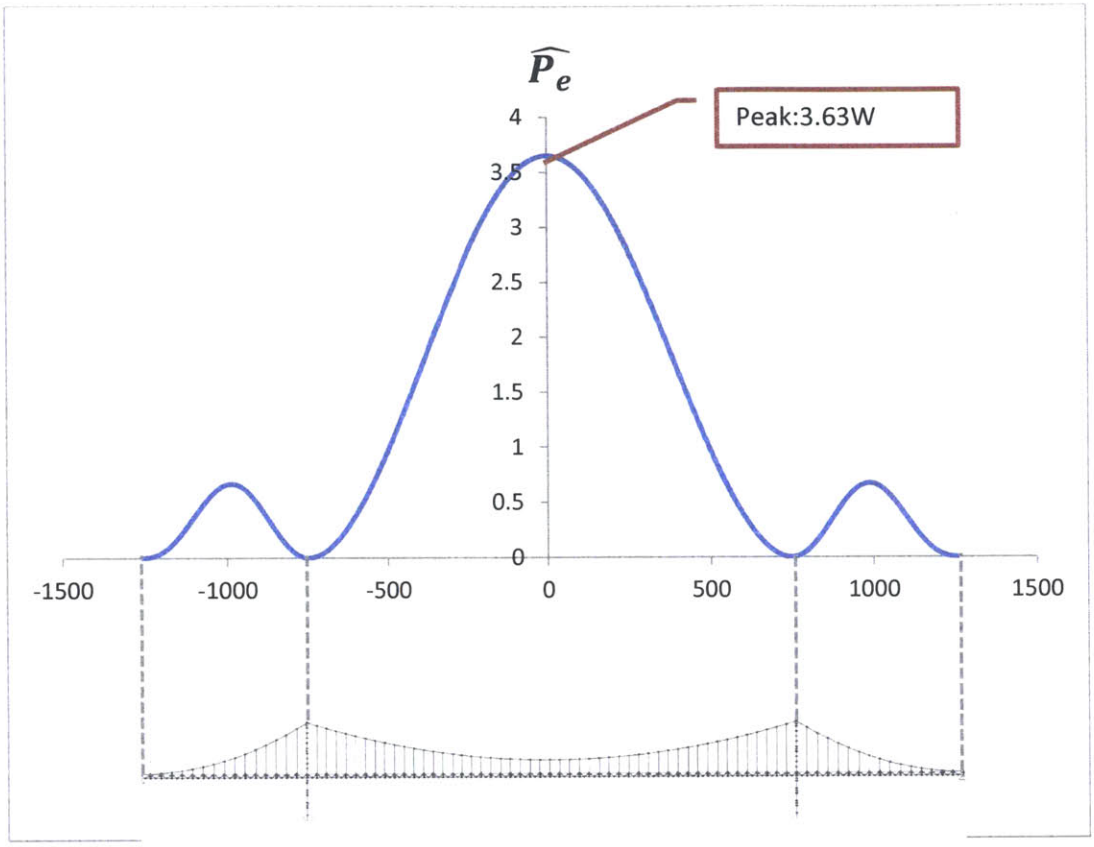

Figure 36 Potential Power Amplitude of the Mass of the Energy Harvester Installed along the Bridge for Equivalent Damping of 0.04

Comparing the two cases for different main structure damping coefficients (0.02 and 0.04), the damping is doubled. The number of energy harvesting devices per panel increased by 25 times, from 30 to 735, and the potential energy harvested increased by 123 times, from 616W to 75.1kW. The cost of the device will also dramatically increase in achieving mechanical damping from 0.00038 Ns/m to 0.00018Ns/m. A study can be done to optimize the cost effectiveness of using energy harvesting devices by adjusting the damping ratio, the amount of energy harvested and cost of the device used.

Chapter 6 Conclusion and Discussion

In this thesis, the oscillation of the suspension bridge deck due to the wind was studied first, with the help of finite element software SAP2000. Then an electromagnetic energy harvesting device is developed to collect energy from bridge deck vibration. The advantage of the device used is its size (2kg, 40mm diameter), which makes it portable. An array of such a device mounted to the bridge deck, not only can harvest energy, but also can control the vibration of the bridge.

Upon analysis, the total energy can be harvested from a 2% total damping is 616W. It can be used to power up the LED board along the bridge. While the energy can be harvested from a 4% total damping is 75kW, which could be used for lightings along the bridge.

The limitation of the device is its frequency range. In reality, the vibration of the bridge can be due to several different sources. Vibration can be induced due to wind, which can excite several modes, and the vibration induced by other sources such as traffic. Different methods to increase the bandwidth of the energy that can be harvested should be studied further.

Another limitation of the direct usage of the harvested energy is the stability of the energy source. The vibration of the bridge deck is influenced by many factors. A proper way to deal with this is the use of energy storage devices, to control the energy output. Then the design of such storages needs to account for the fluctuation of the energy harvested and its location along the structure.

Another important fact is the cost of the device, in order to achieve the maximum energy output the mechanical damping ratio is relatively small, which in turn results increasing the cost of the device. Furthermore, optimizing the cost of the harvesting devices can be studied by reducing the cost of each unit used while attaining a reasonable amount of harvested energy.

Reference

[1] *Energy-harvesting chips: The quest for everlasting life*. (2005, 10 3). Retrieved from EET Asia: http://www.eetasia.com/ART_8800378146_765245_NT_27d01882.HTM

[2] *Shell says record profits to be used to boost alternatives*. (2006, 02 02). Retrieved from Deutsche Presse-Agentur.

[3] *World's First Batteryless Wireless Doorbell*. (2006). Retrieved from Augreener Electronic Technology Co.,Ltd: http://batteryfreedoorbell.en.ec21.com/World_s_First_Batteryless_Wireless--7057319_7098609.html

[4] *U.S. Energy Information Administration (EIA) International Energy Statistics* . (2010, 01 12). Retrieved from U.S. Energy Information Administration (EIA): http://www.eia.gov/cfapps/ipdbproject/IEDIndex3.cfm

[5] *Wikipedia*. (2013, April 22). Retrieved April 28, 2013, from Wikipedia: http://en.wikipedia.org/wiki/Smart_material

[6] Beeby, S. P., Tudor, M. J., & White, N. M. (2006). Energy harvesting vibration sources for microsystems applications. *MEASUREMENT SCIENCE AND TECHNOLOGY*, R175–R195.

[7] Chalasani, S. (2008). A survey of Energy Harvsting Sources for Embeded Systems. *Southeastcon* (pp. 442-447). Huntsville, AL : IEEE Southeastcon.

[8] Connor, J. J. (2002). *Introduction to structural Motion Control.* Cambridge: Pearson Education.

[9] Cooper, J. D. (1998). World's Longest Suspension Bridge Opens in Japan. *Public Roads, Federal Highway Administration.*

[10] *Disc magnet Ø 40 mm, height 20 mm*. (n.d.). Retrieved from supermagnete: http://www.supermagnete.de/eng/FE-S-40-20

[11] *Energy harvesting*. (n.d.). Retrieved from CEDRAT Technologies: http://www.cedrat-technologies.com/en/technologies/mechatronic-systems/energy-harvesting.html

[12] *FE-S-40-20 supermagnete*. (n.d.). Retrieved from http://www.supermagnete.de/eng/FE-S-40-20

[13] Gerner, M. (2007). Chakzampa Thangtong Gyalpo – Architect, Philosopher and Iron Chain Bridge Builder. *Thimphu: Center for Bhutan Studies* , ISBN 99936-14-39-4.

[14] Gimsing, N. J., & Georgakis, C. T. (2012). *Cable Supported Bridges: Concept and Design.* John Wiley & sons, Ltd.

[15] Green, P. L., Worden, K., Atallah, K., & Sims, N. D. (2012). The benefitsofDuffing-typenonlinearitiesandelectrical optimisation of a mono-stable energy harvester under white Gaussian excitations. *Journal of Sound and Vibration 311*, 4504-4517.

[16] Green, P. L., Worden, K., Atallah, K., & Sims, N. D. (2012). The effect of Duffing-type non-linearities and Coulomb damping on the response of an energy harvester to random Excitation. *Journal of Intelligent Material Systems 0(0)*, 1–16.

[17] Hajati, A., & Kim, S.-G. (2011). Ultra-wide bandwidth piezoelectric energy harvesting. *Applied Physics Letters, V99*, 083105_1-083105_3.

[18] Holmes, J. D. (2007). *Wind Loading of structures (2nd Edition).* Taylor &Francis.

[19] Jeona, Y., Sood, R., Jeong, J., & Kim, S. (2005). MEMS power generator with transverse mode thin film PZT. *Sensors and Actuators A: Physical, Volume 122, Issue 1*, 16-22.

[20] Lallart, M., Pruvost, S., & Guyomar, D. (2011). Electrostatic energy harvesting enhancement using variable equivalent Permittivity. *Physics Letters A 375*, 3921–3924.

[21] Mann, B., & Sims, N. (2009). Energy Harvesting from the nonlinear osiccation of magnetic levitation. *Journal of Sound and Vibration 330(24)*, 6036-6052.

[22] Meadows, D., Randers, J., & Behrens, W. (1972). *Limits to Growth.* New York, NY: Universe Books.

[23] Scanlan, R. (1978). The Action of Flexible Bridges Under Wind, I: Flutter Theory. *Journal of Sound and Vibration 60(2)*, 187-199.

[24] Scanlan, R. H. (1978). The Action of Flexible bridge under Wind, II: Buffeting Theory. *Journal of Sound and Vibration 60(2)*, 201-211.

[25] Shinozuka, M. (2009). *Verification of computer analysis models for suspension bridges.* Irvine, CA: Department of Civil and Environmental Engineering, University of California, Irvine.

[26] Simiu, E. (1986). *Wind Effect on structures.* John Wiley & Sons, Inc.

[27] *Suspension Bridge Diagram.* (n.d.). Retrieved from http://www.mmem.spschools.org/oldsite/grade3science/3.bldg/Suspension.html

[28] Theodorsen, H. (1934). General Theory of Aerodynamic Instability and the Mechanism of Flutter. *NACA Report.*

[29] Valluru, S. H. (2007). *Energy Harvesting from Vibration of a bridge.* Knoxville: The University of Tennessee.

[30] Vokoun, D., Beleggia, M., Heller, L., & Sittner, P. (2009). Magnetostatic interactions and forces between cylindrical permanent magnets. *Journal ofMagnetismandMagneticMaterials321*, 3758-3763.

[31] White, N. M., Glynne-Jones, P., & Beeby, S. P. (2001). A novel thick-film piezoelectric micro-generator. *Smart Materials and Structures*, 10-850.

[32] Williams, C., & Yates, R. (1996). Analysis of a Micro-electric Generator for Microsystems. *sensors and Actuators A:Physical 52*, 8-11.